From Years to Hours: Accelerating Model Refinement

Short title: Accelerating model refinement

Kyu Hyong Park[1)], Jordan C. Rozum[2)], and Réka Albert[1,3)]

1) Department of Physics, Pennsylvania State University
2) Department of Systems Science and Industrial Engineering, Binghamton University (SUNY)
3) Department of Biology, Pennsylvania State University

Corresponding authors: Kyu Hyong Park (kjp5774@psu.edu), Réka Albert (rza1@psu.edu)

Keywords: genetic algorithm, Boolean model, model refinement, model update, abscisic acid induced stomatal closure

Abstract

Network-based dynamic modeling is useful for studying how complex biomolecular systems respond to environmental changes and internal perturbations. The main challenge in constructing a dynamic model is integrating evidence from perturbation (e.g. gene knockout) experiments, because their results arise from the collective function of the regulatory network. For a model to capture these non-local effects, its construction, validation, and refinement necessarily involve trial and error, constrained by domain knowledge.

We propose and implement a genetic algorithm-based workflow to streamline model refinement. This workflow applies to any biological system for which an interaction network and enough perturbation experiments exist. The algorithm we introduce adjusts the functions of the model to enhance agreement with a corpus of curated experimental results and leverages existing mechanistic knowledge to automatically limit the search space to biologically plausible models. To account for the interdependence of experimental results, we develop a hierarchical scoring technique for assessing model performance. We implement our workflow for Boolean networks, which are a popular and successful tool for modeling biological systems, but the workflow is readily adaptable to multi-level discrete models. Our implementation is available as the open-source Python library *boolmore*.

We demonstrate *boolmore*'s effectiveness in a series of published plant signaling models that exemplify the challenges of manual model construction and refinement. These models describe how plant stomata close in response to the drought hormone abscisic acid. After several hours of automatic refinement on a personal computer, the fittest models recapture and surpass the accuracy gain achieved over 10 years of manual revision. The refined models yield new, testable predictions, such as explanations for the role of reactive oxygen species in drought response. By automating the laborious task of model validation and refinement, this workflow is a step towards fast, fully automated, and reliable model construction.

Author summary

Biomolecular networks are quintessential complex systems, wherein the interactions of proteins and molecules give rise to cellular phenotypes. Modeling these systems requires

making choices about the rules governing individual genes and proteins, but often experiments only constrain their effect on the system-level behavior. This contrast presents a challenge to updating an existing model to align with new experiments. The traditional approach to revising a baseline model is essentially trial-and-error. We present a method, implemented as the open source Python library *boolmore*, that leverages recent advances in the computational analysis of discrete dynamical systems to automate this process, reducing a task that often takes years to a matter of several hours on a personal computer. We showcase the power of this method on a model describing how plant leaf pores respond to the drought hormone abscisic acid. This model was first published in 2006 and has been updated several times, by hand, to incorporate new experimental data or to improve model performance. *Boolmore* not only recaptures these refinements, but produces models that better explain experimental results and uncover new insights into the regulatory mechanisms of drought response.

Introduction

Network-based dynamic modeling is an effective avenue toward understanding the response of biological systems to changes in their environment. The system is abstracted into a network, whose nodes represent the components of the system (e.g., proteins, cells, neurons, or species) and whose edges represent the directed, causal interactions among them. The dynamic model assigns each node a continuous or discrete state variable and a regulatory function that determines the future state of the node given the current states of its regulators. Boolean models are the simplest discrete dynamic models. They are used to model a variety of biological systems; examples include gene regulatory networks [1], neuronal networks [2,3], ecological and social communities [4,5]. In Boolean models, the node state variables can take two values, 0 (interpreted as low concentration or activity) or 1 (interpreted as high concentration or activity). Boolean models typically use a discrete and implicit time variable; frequently used implementations are synchronous and asynchronous update, in which every node or a single randomly selected node is updated at each time step, respectively. The biological predictions of models are typically, but not always, robust to the update scheme [6]. Multiple methodologies and tools can determine the possible long-term behaviors of systems described by Boolean models [7–10]. Although the update scheme affects the dynamics of the Boolean model, here we take advantage of minimal trap spaces, which are robust to the update scheme, to describe long-term behaviors of the system. A minimal trap space (also called a quasiattractor) is a minimal set of node states that is closed under the time evolution of the system (i.e., that the system can be “trapped” in) and that can be characterized by fixing the values of some subset of the node state variables. When a minimal trap space is characterized by fixing all node state variables, then it corresponds to a fixed point attractor; if, on the other hand, some node state variables are not fixed, then the minimal trap space contains a complex attractor in which the unfixed variables may oscillate.

Boolean models are especially suitable for biomolecular networks due to the abundance of nonlinear, sigmoidal regulation in these networks [11,12], and because of these models’ ability to describe perturbation (e.g., genetic knockout) experiments. Through integrating the knowledge of the biology community, Boolean models successfully capture key behaviors in the biomolecular system of interest, and make useful predictions such as identifying master regulators or drug targets. An example of the former is a Boolean model of T cell differentiation in response to the cellular microenvironment whose 22 point attractors

could be grouped into 8 documented T cell types such as helper and regulatory T cells [13]. An example of the latter is a Boolean model of the cell fate change that represents the first step toward metastasis in liver cancer, which identified the interventions that are able to prevent or reverse this fate change [14]. Predictions derived from Boolean models for a variety of biological systems were verified experimentally [15,16].

Due to recent advances in the analysis of Boolean dynamics [10,17–19], the bottleneck in analyzing a biomolecular system is increasingly the time and effort involved in building the model itself. When full state data (i.e., the state of all the components at a given time) is available, there are several viable automated Boolean network inference methods available [20–25]. However, in many systems there are no high-throughput assays that can be used to obtain such comprehensive data and the information-gathering is instead piece-wise. In this case, integrating all the relevant experimental evidence from publications is a challenge. Experimental observations of interactions (e.g. chemical reactions and protein-protein interactions) and positive or negative regulation (e.g. transcriptional or allosteric regulation) informs the edges of the network. Another type of experimental evidence is a single observation that is nevertheless influenced by the whole system (e.g., it indicates that the knockout of a gene impairs the system's response to a signal). It is not possible to directly assimilate this type of global evidence into any individual node's regulatory function, as the function only incorporates the effects of the node's direct regulators (i.e., it is purely local). Although some parts of the model can be directly constrained by preexisting experiments, usually many degrees of freedom remain. Fully exploring the space of all regulatory functions that are consistent with local information and systematically testing the agreement of the resulting model with global system-level data is prohibitive. In practice, modelers often tackle this challenge through a process of trial and error informed by the insights of domain experts.

Keeping the model up-to-date involves the same trial and error iteration. Experiments performed after the construction of the model may disagree with the model, or identify important new elements that the modeler would like to capture in the model. For example, the earliest version of a model of T cell differentiation, introduced by Luis Mendoza, initially had 17 nodes and reproduced the three T helper cell types known at the time [26]. After the identification of T regulatory cells, the model was expanded to 35 nodes [27] and reproduced five T cell types. After a significant expansion to 85 nodes, and a subsequent logic-preserving reduction, the model reproduced eight T cell types [13].

An illustrative example of the time and effort needed for model construction, validation, and update is the Boolean model of abscisic acid-induced stomatal closure in the model plant *Arabidopsis thaliana*, which was introduced and refined in [28–31]. This model describes how the hormone abscisic acid (ABA) induces the relaxation of plant guard cells and subsequent closure of stomata. Stomata are microscopic pores on the leaves through which the plants take in CO_2 necessary for photosynthesis and through which the plant inevitably loses water. The stomata open in response to environmental signals such as light. ABA is a stress hormone that is produced when the plant is dehydrated, and its role is to help the plant conserve water. ABA acts as a signal in a network of protein interactions, enzyme-catalyzed reactions and ion flows, whose ultimate effect is stomatal closure. Understanding this network provides an avenue for gaining insight about the regulatory mechanisms underlying drought tolerance, which is of paramount importance for plant survival and crop resilience. The variety of processes involved in this network also exemplifies the potential complexity of the signal processing of living systems. The first version of this Boolean model of ABA-induced closure was developed starting in 2003 and

was published in 2006 [28]. At that time, the receptor proteins to which ABA binds were not known. Following the identification and confirmation of the RCAR receptor family [32–34], the ABA-induced closure model was significantly expanded in the period 2014-2016 and an updated version was published in 2017 [29]. The 2017 version of the model was subsequently improved in 2019 to better account for the possibility of stomatal closure in response to intracellular stimuli [30] and then in 2020 to reproduce the reversibility of stomatal closure [31].

Our aim is to speed up and automate the trial and error process needed for model validation and refinement. Specifically, we consider the problem of refining and updating an existing baseline model to better agree with existing experimental data and also incorporate new data. We assume that the baseline model has a relatively complete interaction network, missing perhaps only a few edges. We develop a genetic algorithm-based workflow to adjust the update functions of the model in a manner that optimizes the model's agreement with curated experimental results. The workflow, and its implementation in the tool *boolmore* (BOOLean MOdel REfiner), includes multiple ways to incorporate biological expertise that can limit the genetic algorithm's search space to models that agree with biological knowledge. We demonstrate the effectiveness of our workflow by generating refined models of ABA-induced stomatal closure that agree significantly better with a compendium of published experimental results than the previous models.

Methods

We propose and implement a genetic algorithm-based workflow to systematically tackle the huge number of modeling choices and experimental results that must be considered during model validation and refinement. Genetic algorithms are a type of heuristic optimization that produce candidates through stochastic mutation and retain or eliminate them depending on a fitness score [35]. In the context of the problem considered here, the sought-after solution is the optimal refinement of an existing Boolean model (which consists of a signed interaction graph and the Boolean functions of each node). Our proposed model refinement tool, called *boolmore*, uses the starting model to build a large number of mutated offspring models that are consistent with the interaction graph (unless otherwise specified) and with modeler-specified biological constraints but that have different regulatory functions. *Boolmore* scores the fitness of each model by comparing the model's predictions to a compendium of experimental results. The encoding of the experimental results and the scoring functions are designed to combine biological realism with flexibility, as described in detail in later sections. *Boolmore* is meant to be used in conjunction with domain expertise to interpret the refined model and extract new predictions from it.

The previous works most relevant to our method involve genetic-algorithm-based inference of a Boolean model based on a directed network that integrates prior knowledge of interactions and regulatory relationships [21–25,36] These algorithms take as input information a compendium of steady state values of all the nodes in the unperturbed system, complemented by the steady state values obtained for perturbations. Another type of relevant prior work develops answer-set-programming methods to revise an existing Boolean model to better align with steady state or time course measurements of the unperturbed system [37,38]. We summarize in S2 Text the goals and use cases of relevant previous algorithms. All of these approaches require system-wide steady state or time course information, such as high-throughput gene expression (transcriptomics) or protein expression (proteomics) experiments. In contrast, many biological publications focus on a

single outcome (for example, stomatal closure) or a single variable (for example, the level of a single protein) and report the changes to this outcome in response to various signals and interventions. Due to the lack (and often impossibility) of simultaneous measurements of all elements of the system, the system's steady states are often not known, and consequently the existing methodologies cannot be used. Of the methods considered in S2 Text, our workflow is the only viable automated approach when high-throughput measurements are not available. Previously, the only way forward in such settings was to manually incorporate hand-curated experimental data into a model, a laborious process that relies heavily on domain expertise due to the enormous search space.

As is common practice in network inference, we demonstrate the performance of *boolmore in-silico* using artificial input data constructed from the dynamics of existing Boolean models.The models refined by *boolmore* showed a 95% success rate in predicting the outcome of new artificial experiments (see Results). In addition, we showcase our workflow in a case study using previously published biological experiments and model refinements.

Outline of the *boolmore* tool

The model refinement process of *boolmore* repeatedly iterates through the steps depicted in Figure 1. First, it mutates the functions of the starting model to form new models, as described in detail in S3 Text. The mutation is constrained to preserve all the knowledge in which there is high confidence, for example the sign of each edge, which represents positive or negative regulatory influence. Every edge can be deleted and later recovered. Edges not in the original network can be added from a user-provided pool. *Boolmore* also generates crossover models in which each node's regulatory function is randomly chosen from one of two models. Second, the predictions of the models are generated. We use *pyboolnet*, a Python package for analyzing Boolean models [17] to determine the minimal trap spaces of the model under various constraints that mimic experimental settings. Minimal trap spaces are a close, update scheme independent approximation of attractors and their identification is more computationally efficient (see S1 Text). For each minimal trap space, nodes constrained to be ON are assigned the value of 1, nodes constrained to be OFF are assigned the value of 0, and unconstrained nodes are assigned the value of 0.5. We take the average of the assigned value for each node over all minimal trap spaces in a certain setting as the prediction of the model in that setting. Third, as described in detail in the following sections, *boolmore* computes the model's fitness score by quantifying the agreement of the model predictions with multiple related experiments such that more biologically reasonable models obtain higher scores. Finally, *boolmore* keeps the models with the top 20% of fitness scores, while also preferring models with fewer extra edges compared to the original.

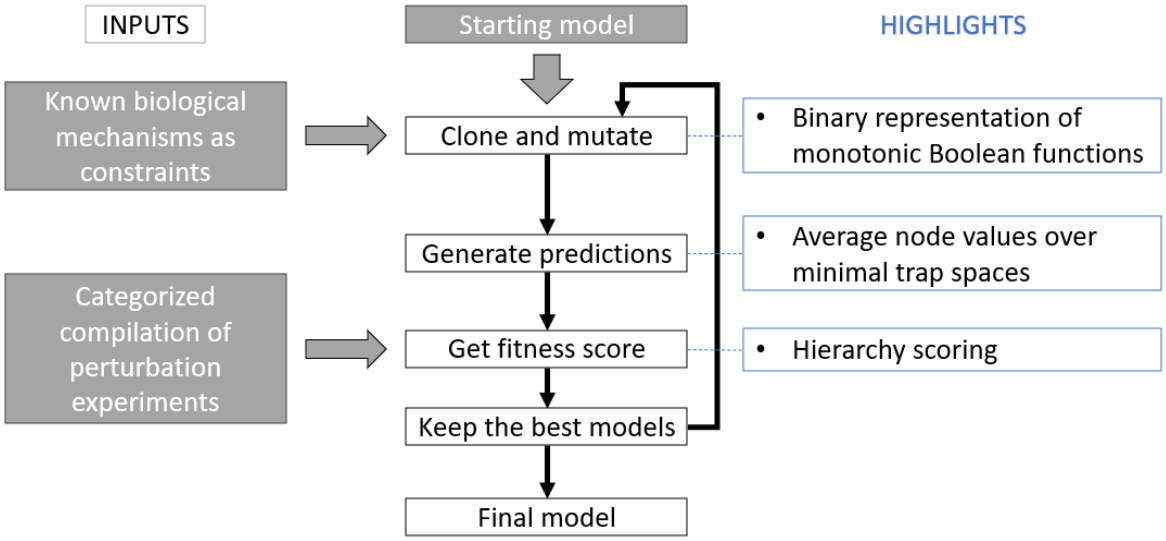

Figure 1. The outline of the *boolmore* tool. The starting model, known biological mechanisms and a categorized compilation of perturbation experiments are taken as input. These inputs are integrated directly into the model refinement process, as they are used to generate and score every single model. We introduced a new representation to allow the mutation of Boolean functions while maintaining consistency with the interaction graph and the biological constraints. *Boolmore* finds the predictions of the models through the minimal trap spaces and uses hierarchy scoring to ensure that reasonable models receive higher scores.

Our workflow and implementation in *boolmore* exhibit several innovative features such as a hierarchical grouping of experimental results and a new representation of monotonic Boolean functions that facilitates generating mutations that preserve edge sign. We describe these key features in the following subsections.

Interpreting experimental results in a Boolean context

Boolmore computes each model's fitness score using input data consisting of experimental interventions and a coarse-graining of the corresponding experimental outcomes. We used five categories of experimental results for each node: OFF, OFF/Some, Some, Some/ON, ON; we describe below how we assigned these categories, though we note that our workflow is flexible and allows other choices.

Experimental interventions such as knocking out a gene or providing excess amounts of a protein have natural Boolean interpretations; the corresponding nodes are considered to be fixed OFF for the former and ON for the latter. The observations of mRNA or protein concentrations in the unperturbed (wild type) or perturbed (e.g., mutant type) systems have a continuous spectrum of outcome. We use a comparative method to express these outcomes in a form that is compatible with Boolean dynamics. In the case of a signal transduction network, we use the levels of activation of the nodes in the presence/absence of the signal (in the wild type system) as two points of reference, akin to a positive and negative experimental control. We coarse-grain node activities in response to interventions by comparison to these two points of reference.

We illustrate in Figure 2A the case of a node R, which has higher activation when the signal S is present in the wild type. We consider this level of activation to be the ON state (R=1), and in any intervention that leads to a similar activation level or higher, R is considered ON. The levels are assigned to the OFF state in a similar manner. In addition to

the preferred OFF and ON categories, we also introduced intermediate and mixed categories as necessary. If the activation level is an intermediate between the OFF and ON states, it is categorized as “Some”. Although a Boolean model has no simple way of describing such an intermediate level, it can be realized by an attractor in which the node oscillates or by multiple attractors, with the node being with ON in some of the attractors and OFF in the others. We discuss the interpretation of the “Some” category and its possible customization in S4 Text. We assigned the OFF/Some or Some/ON categories in cases when there are multiple reported experiments for the same intervention that have non-identical results, or in cases where a clear comparison with the reference was impossible. The next section describes the way in which this categorization is used to score the models.

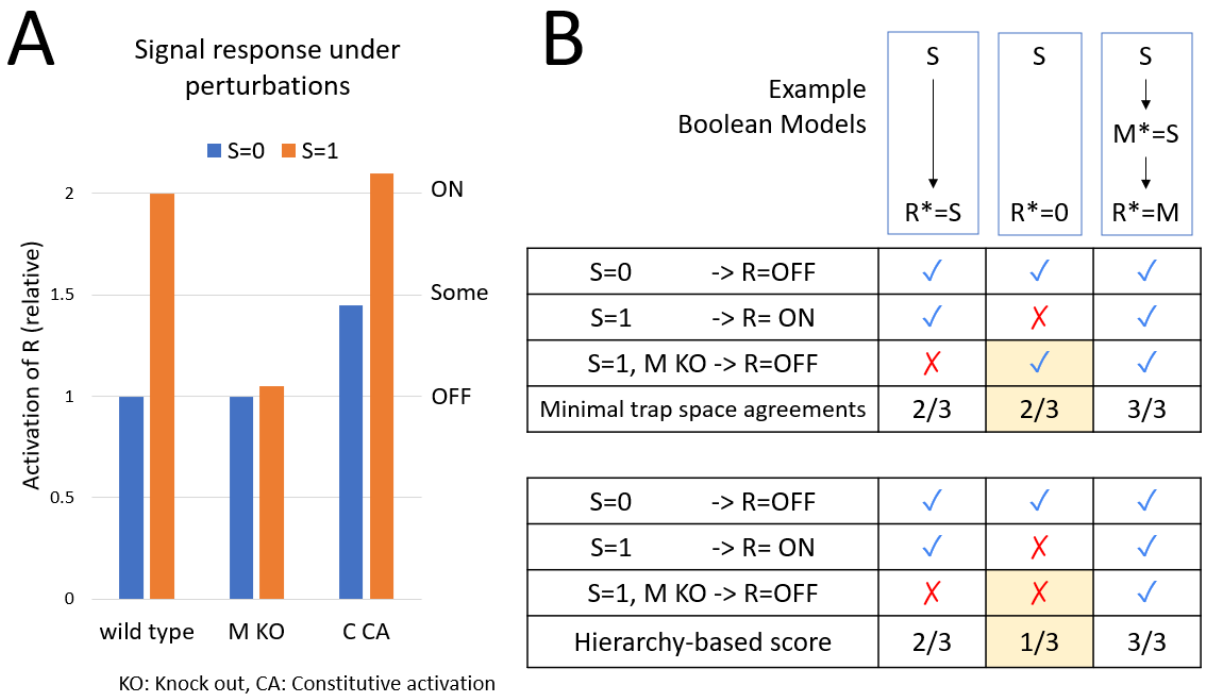

Figure 2. (A) Illustrative example of perturbation experiments. The reported results are normalized by the activation of the response node R in the absence of the signal (S=0). The wild type shows higher activation of R in the presence of the signal S. M and C represent mediators of the signal.”KO” means knockout and “CA” means constitutive activation, thus “M KO” refers to M=0 and “C CA” refers to C=1. The wild type response under S=0 is categorized as OFF; the wild type response under S=1 is categorized as ON. If the value of R obtained under a perturbation is similar to one of these two reference values, it will be included in the same category as the reference. For example, the response to [S=1, C=1] is categorized as ON. Notably, the response to [S=0, C=1] is categorized as Some. (B) Illustrative example of determining the minimal trap space agreement and the hierarchy-based score of putative models. Each model indicates the next state of R (denoted R*) as a function of the current state of S or M. The model with R*=0 has the same minimal trap space agreement as the R*=S model, but it receives a lower hierarchy-based score because of its discrepancy with a wild-type experiment. In general, the difference between the minimal trap space agreement and the hierarchy-based score (highlighted in yellow) is more prominent in more complex perturbation experiments.

Scoring model fitness with a hierarchy-based method

Each model receives one point toward its fitness score per recapitulated perturbation experiment outcome. To ensure that the simulated intervention is causally linked to the model outcome, a perturbation experiment is considered to be recapitulated only if the model predictions agree with measurements obtained for subsets of the perturbation as well, resulting in a hierarchy of experimental observations. The top of the hierarchy is the 'resting state' observation of the wild type system in the absence of any signal. The signal-response pairs of the unperturbed (wild type) system are one step down, as are the responses to perturbations of single intermediary nodes in the absence of any signal. The signal-response pairs under perturbations of single mediators are two steps from the top. Perturbations of multiple mediators are at increasingly lower levels of the hierarchy.

As an illustrative example, consider a system in which a signal S leads to a response R through a mediator M (see Figure 2B). The knockout of the mediator (M=0) inhibits the response to the signal (R=0 even if S=1). A hypothetical model that says R is inactive regardless of the signal (R*=0) recapitulates the result that M=0 leads to R=0. However, this model does not respond to the signal even when M=1. Our scoring method ensures that a high-scoring model satisfies the top-of-the-hierarchy experiment [S=0]→R=0, the one step down experiment [S=1]→R=1, as well as the more complex experiment [S=1, M=0]→R=0. Note that S=0 is the default and should be included in the specification of the experiment unless S=1.

Boolmore scores each model in a two-step process. First it determines the agreement of the model with each perturbation experiment, and then it scores the model by considering all agreements with the experiments at higher levels of the hierarchy. For each perturbation condition, the model prediction is the average value of the observed node in the minimal trap spaces (see S3 Text). The model's agreement for that perturbation experiment is given depending on how well the prediction agrees with the categorization of the experimental outcome. Each agreement function's output ranges from 0 to 1 (see S1 Table). For example, if the experimental outcome is categorized as ON, a model with a prediction of 1 receives an agreement of 1 for that experiment and another model with a prediction of 0.5 gets an agreement of 0.5. The final score is the product of all the attractor agreements of the subset perturbation experiments. For example, in Figure 2B, if we are considering the perturbation [S=1, M=0], the score is given by multiplying the agreements of 3 experiments, namely [S=1], [S=0, M=0], and [S=1, M=0] itself. Going back to our previous example, the model with R*=0 has an agreement of 1 for the experiment [S=1, M=0]→R=0. However, as its agreement for [S=1]→R=1 is 0, it will not receive a score from this experiment.

Mutating functions such that edge signs are preserved

To ensure that the model improvement process preserves the sign (positive or negative effect) of each interaction, we devised a degenerate binary representation of each function based on a disjunctive normal form of the function. A function with p positive regulators and n negative regulators can be expressed (not necessarily uniquely) as the disjunction (OR composition) of a subset of the 2^{n+p} conjunctions (AND compositions) consistent with the regulatory signs. Each of these conjunctions is assigned a location in a binary string of length 2^{n+p}; the binary string is interpreted as the disjunction of the conjunctions corresponding to the locations in which the string has a 1. Each mutation changes a randomly selected digit of this binary representation and is guaranteed to preserve the signs of the regulatory relationships (see S3 Text). To remove bias toward one output state or the

other, we introduce a 50% chance to mutate the negation of the function rather than the function itself.

Preserving known mechanisms via constraints

In some cases, the biochemical mechanisms of certain regulatory relationships are known. We encode such knowledge as constraints to the regulatory functions, in a similar vein as [39]. These constraints not only ensure reasonable models, but they also reduce the search space greatly. For example, if it is known that the activation of a regulator A is sufficient for the activation of the target B, then the form of the update function of B is constrained to be "B*= A OR (other regulators)". For a function with 4 inputs, this reduces the number of possible Boolean functions with fixed signs from 168 to 20. We implemented five types of constraints in our case study described in the Results. The currently implemented constraints are based on our current experience with using *boolmore* on a signal transduction network. Future applications will likely reveal new constraints, which can be implemented.

Allowing the addition of new edges from a limited pool of experimentally-supported hypotheses

Boolmore modifies the interaction graph by deleting or adding edges. The deletion of edges is done implicitly through the modification of regulatory functions. The addition of edges was implemented in a restrictive way: *boolmore* can only select edges from a predetermined pool. Initially, the new regulator is integrated with the rest in a random way (see S3 Text), and the function can mutate through the iterations. Models are given internal penalties when adding edges, so that models in which the addition of an edge did not lead to a score increase are less likely to survive through the iteration. This method helps prevent the models from deviating too much from the original interaction graph and from increasing their complexity. However, even with these preventive measures, each edge in the pool makes the search space exponentially larger, and can preclude the algorithm from finding an optimal model in a reasonable amount of time. Hence we only allowed the addition of user-provided edges, often limited to edges with experimental support.

Results

We show benchmark results to demonstrate the performance of *boolmore* on randomized versions of 40 previously published models using synthetic data. We also present a case study on the ABA-induced stomatal closure model [29], proving that our tool is highly effective in a real model refinement process. As we describe in this case study, the new and improved versions of the model led to testable biological predictions.

Benchmark analysis to test the overall performance of *boolmore*

First, we demonstrate the performance of our algorithm through benchmark studies. Following the common practice in such benchmarks, we used existing Boolean models to generate artificial experiments. We used 80% of the artificial experiments as the training set to refine a randomized starting model generated using the original model's interaction graph; we used the remaining 20% as the validation set to test the accuracy of the refined model in recapitulating newly encountered experimental results.

We used 40 Boolean models in the Cell Collective (a repository of peer-reviewed, experimentally supported Boolean models [40]) and ran 5 replicate benchmark runs for each of them. We selected models with fewer than 30 nodes. For each model with N nodes, we generated five sets of 10*N artificial experiments, 80% of which were used for training, for a coverage that is comparable to that of our case study (505 experiments for 68 not fully constrained nodes). Each artificial experiment consists of a set of nodes whose state is controlled (kept fixed) and a node whose state is observed. The controlled set of nodes always included the source nodes of the network; each non-source node had a 1/N chance of also being included. The observed node was one of the sink nodes or, with a lower priority, it was a randomly selected node. We fixed the values of the nodes in the controlled set randomly and determined the average node value of the observed node in the minimal trap spaces. Depending on the average value, the result was classified into one of the 5 categories described previously, using thresholds that ensure that the original model would have a perfect fitness score.

We generated five starting models for each model by randomizing the binary representation of the update functions of the original model. This randomization keeps the functions monotonic and consistent with the original interaction graph, but may yield fewer regulators than the original. The missing regulators can be added back in during the iterations of the algorithm. We used *boolmore* to refine the models over 100 iterations and score them by comparing their results to the results of a subset (80%) of the artificial experiments following the procedure described in the Methods.

We found that the starting models had on average 49% accuracy on the training set, and *boolmore* improved them to 99% accuracy on average (Figure 3). Notably, *boolmore* also increased the accuracy of the models on the validation set from 47% on average to 95% on average. This indicates that *boolmore* does not overfit the training set and that the refined models can give valid predictions.

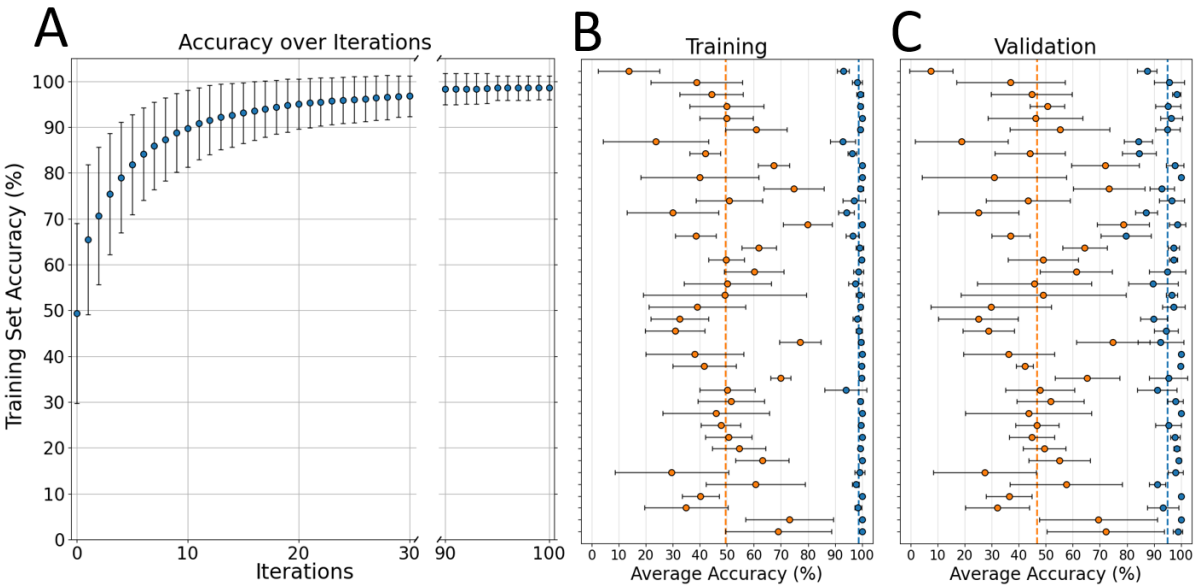

Figure 3. (A) Illustration of the accuracy improvement on the training set (80% of the artificial experiments) over the iterations of the algorithm. The blue circles represent the average accuracy of the 185 model variants at each iteration, and the error bars represent the standard deviation. (B) Results of benchmark studies using an ensemble of 40 published Boolean models. For each model the average accuracy on the training set (80% of artificial experiments) of the 5 starting model variants is shown in orange, and the average accuracy

of the 5 refined models is shown in blue. Error bars represent the standard deviation across the 5 replicates. The names of each model and their accuracies are listed in S2 Table. Orange and blue dashed lines indicate the average accuracy of the starting models (49%) and the refined models (99%) respectively. (C) The average accuracies on the validation set (20% of artificial experiments) of the 5 starting model variants (orange) and the 5 refined models (blue). *Boolmore* had no information on the validation set in its model refinement process, but was still able to improve the accuracy greatly, from 47% on average to 95% on average.

Case study: improving the ABA-induced stomatal closure model.

To go beyond simple benchmarks and use our approach to search for new biological insights, we apply our method in a case study. We selected a system that is representative of the challenges inherent in constructing a Boolean model of a complex biological phenomenon and keeping it up-to-date with current literature. Specifically, we analyzed a group of Boolean models, each aiming to integrate the mechanisms through which the hormone ABA leads to the closure of stomata. These mechanisms include activation of enzymes, production of molecules such as reactive oxygen species (ROS), nitric oxide (NO), and phosphatidic acid (PA), transient increases in the cytosolic Ca^{2+} level (Ca^{2+}_c) due to Ca^{2+} flow through the membrane (CaIM) or to Ca^{2+} release from stores (CIS), and ion flow across the cellular membrane. The first model of ABA-induced closure, published in 2006 by Li et al. [28], included 42 nodes. This was expanded to 81 nodes in 2017 by Albert et al. [29]. An alternative expansion to 60 nodes was published in 2018 by Waidyarathne and Samarasinghe [41]. The 2017 model was refined in 2019 by the addition of a new edge and a simultaneous attractor-preserving reduction to 49 nodes [30]. We decided to use the 2017 model as the basis of model refinement, as it is the most comprehensive and its analysis included a thorough comparison with experiments.

The full and abbreviated names of all the elements included in the 2017 model are listed in S3 Table. One notable feature of the model is that it includes a negative feedback loop between the node Ca^{2+}_c, which represents an increase in the cytosolic level of Ca^{2+}, and the node Ca^{2+}ATPase, which represents the pumps and channels that decrease the cytosolic Ca^{2+} level to avoid damage to the cell. This negative feedback loop leads to an irregular Ca^{2+}_c oscillation in the model in the presence of ABA, which represents the transient Ca^{2+}_c increases of the real system [42]. The attractor of the model in the presence of ABA features the sustained state of 71 nodes (including the outcome node Closure) and the oscillating state of 10 nodes (including Ca^{2+}_c and Ca^{2+}ATPase). Albert et al. used simulations to classify perturbations (e.g., genetic or pharmacological knockouts, constitutive activation of elements) into five categories in terms of the closure response to ABA: close to wild type response, hypersensitivity (faster closure), hyposensitivity (slower closure), reduced closure, and insensitivity to ABA (i.e., lack of closure). When comparing model results and experimental results, any defects in closure were considered consistent with each other. Based on a comparison with 112 perturbation experiments, the reported accuracy of the model was 95/112=85%.

Despite the overall high accuracy, the model also exhibited two important weaknesses. First, there are 9 nodes that were shown experimentally to lead to closure when activated by external interventions, as did one node knockout. The 2017 model failed to recapitulate nine of these results according to the simulation-based criteria used at the time. Second, plant stomata reopen after the removal of the ABA signal, enabling the plant

to resume photosynthesis. This reversibility of stomatal closure is not captured by the model. This is because there is a single attractor with Closure=1 out of 17 attractors in the absence of ABA. After the model converges to the closure attractor in response to ABA, the removal of ABA will lead to this single attractor, and not cause loss of closure.

Two follow-up publications aimed to address each of these two weaknesses of the 2017 model by making parsimonious hypotheses. Maheshwari et al. [30] hypothesized in 2019 the existence of an additional edge. They found that the model augmented by an inhibitory edge starting from cytosolic Ca^{2+} and targeting any of four PP2C phosphatase family members recapitulates five of the nine experimental observations of closure that were not captured by the 2017 model. They confirmed this inhibitory effect by experimentally observing a decrease in PP2C phosphatase activity in response to externally provided Ca^{2+}. Considering the possibility of this effect being indirect, Maheshwari et al. also demonstrated that it could be mediated by PA with very similar model results.

The 2019 model [30] shared the irreversibility of stomatal closure exhibited by the 2017 model. A second follow-up to the model in 2020 [31] identified that the source of irreversibility is the assumption of self-sustained activity of four nodes regulated by Ca^{2+}_c. This assumption was made in the 2017 model because if the activity of these four nodes would decrease when Ca^{2+}_c decreases then sustained closure would not be possible. The 2020 model incorporated the additional edge introduced in the 2019 model and made the regulatory function of these four nodes time-dependent. This time dependence serves as a memory of past Ca^{2+}_c increase that makes the activity of these nodes less likely to decrease, making the assumption of their self-regulation unnecessary. The 2020 model achieved reversible closure and preserved the 2019 model's success in capturing five of the experimental observations of closure in response to interventions. We emphasize that both of these improvements were proposed after an in-depth analysis of the 2017 model's weaknesses and individual exploration of many possible hypotheses to address these weaknesses while preserving the strengths of the model.

We aimed to refine the 2017 model and improve its agreement with the corpus of experiments performed for ABA-induced closure, while also reproducing the results of the manual improvement process described above. We undertook an extensive search of the experimental literature and expanded the number of experimental observations to 505 (see S4 Table). We re-evaluated the 2017 model using the minimal trap space-based criteria more suitable for fast evaluation of many models. With this evaluation, the 2017 ABA model showed a score of 310.5/505 (61.5%). The decrease in score compared to the original evaluation of the model is due to several factors: our compilation of experiments is larger, our evaluation also uses observations of nodes other than closure, and our scoring criteria are different. We had three main goals for the improvement of the model: achieving better overall accuracy, achieving closure by the documented key interventions, and achieving reversibility of stomatal closure.

Correcting an error and choosing baseline models

The original 2017 model had an erroneous edge between the node Vacuolar Acidification and the node KEV, which represents vacuolar K^+ channels necessary for the ion flow that precedes stomatal closure; the inaccuracy of this edge was recognized in a later publication [43]. We found that the model corrected by deleting this edge had a low accuracy (see the second row of S5 Table), and was unable to recapitulate sustained stomatal closure in response to ABA. The reason for this failure is that the sole remaining regulator of KEV, Ca^{2+}_c, oscillates, leading to oscillating closure. We attempted to fix this discrepancy using

boolmore. Although the algorithm achieved a score improvement (see the third row of S5 Table), it was unable to achieve sustained activation of closure in response to ABA. This shows the importance of having a good starting interaction graph for our workflow. To have a starting model that recapitulates the core behavior of ABA-induced closure, we pursued two ways to eliminate the spurious oscillations in the output node Closure.

First, drawing inspiration from the 2017 model, which assumed self-sustained activity of four nodes that would otherwise exhibit Ca^{2+}_c-driven oscillations, we introduced a self-edge to the abstract process node "H_2O efflux" (see S5 Text for more detail on this decision). The improved regulatory function expresses the assumption that water efflux, once started, can be sustained even if K^+ efflux stops, if all other conditions continue to be met. This model recapitulated ABA-induced closure and had a score of 311.7/505 (61.7%). We adopted this model as the first baseline model (A).

Second, in an alternative approach, we introduced a global, qualitative change to the 2017 model by implementing a different representation of the dynamics of cytosolic Ca^{2+}. The literature on ABA-induced stomatal closure includes significant debate regarding the role of cytosolic Ca^{2+} [42,44]. Substantial spatio-temporal variability was observed, including spatial hotspots, transients, spikes, and oscillations [42]. The emerging conclusion is that cytosolic Ca^{2+} elevation plays an amplifying role in ABA signaling [45]. Nevertheless, there is no consensus on whether the return from the elevated Ca^{2+} level has a regulatory role (in other words, whether it matters if Ca^{2+} has one or multiple increases). In the original and the baseline A model, the oscillation of Ca^{2+}_c drives 10 nodes into an oscillating state. In contrast, the existing experimental observations of 32 elements in response to ABA only indicate an oscillatory activity for Ca^{2+}_c. We note that many assays observe a population of guard cells at a single time point; such assays can neither rule out nor support oscillations of certain elements at the level of individual guard cells. As an alternative to the self-sustained activation of Ca^{2+}_c targets assumed in the 2017 model and in the baseline A model, we replaced the two-node negative feedback loop with a single node, 'Ca^{2+}_c osc', whose ON state represents the appearance of Ca^{2+} elevation transients and whose OFF state represents an unchanged low cytosolic Ca^{2+} level. We also deleted the four assumed self-edges. The replacement of an oscillating node with a non-oscillating one is a potentially dramatic change because it stabilizes the positive regulation and positive feedback loops in the system. Indeed, this model only had point attractors. We found that the thus-modified model had a score of only 184.2/505 (36.5%), mainly because it did not recapitulate the reduction of ABA-induced closure for single-node interventions. We adopted this model as our second baseline (B), aiming to find out whether a model that lacks oscillations can reach equal agreement with the experimental observations.

In our application of the genetic algorithm on either baseline model, we adopted specific constraints and criteria for allowing additional edges, as we describe next.

Constraints and pool of additional edges

We use four types of constraints: fixed functions, edge preservation, logic preservation, and grouped regulation.

We apply the fixed function constraint to 13 nodes, which prevents their update functions from mutating. These thirteen update functions of the 2017 model express known biochemical reactions or biophysical mechanisms with especially firm and direct evidence. One such example of a fixed function is cADPR* = NAD^+ and ADPRc. This function describes the sole reaction in which cADPR (cyclic ADP ribose) is produced in this system; the reactant of this reaction is NAD^+ and it is catalyzed by ADPRc (ADP-ribosyl cyclase).

Apart from fixing these 13 update functions, we also enforce that 9 additional edges are preserved. These are 9 cases of regulator-target pairs that have direct experimental evidence but insufficient evidence to constrain how the regulator is coupled to the other regulators of the target. The edge preservation constraint ensures that the update function of the target node always contains the regulator as a non-redundant input. One such example is the AnionEM→Depolarization edge, which indicates that the efflux of anions promotes the depolarization of the plasma membrane. Every version of the regulatory function of the node Depolarization must contain AnionEM. We also prevent each node from becoming a source node due to edge loss. The exception is GEF1/4/10, which is a source node in the original model but can acquire (and later lose) a new edge from the pool.

We preserve the logical role of 6 additional edges. For these regulator-target pairs, it is known that the activity of the regulator is necessary for the activation of the target. We require that any modification of the function of the target node preserves this necessity. One such example is the necessity of the enzyme activity of RBOH (respiratory burst oxidase homolog) to produce reactive oxygen species (ROS node). A regulatory function of the type ROS* = RBOH and X, where X is an additional regulator of ROS, reflects the necessity of RBOH for the production of ROS.

Finally, we impose a grouped regulation constraint to four groups of nodes. In these cases, it is known that a specific enzyme-catalyzed reaction may contribute to the production of a molecule, but additional possible reactions or regulatory effects allow flexibility to the function. For example, three separate reactions were identified as potentially contributing to the production of PA during stomatal closure, but the relative contributions of these reactions are not known. The 2017 model assumed that each of the three reactions is independently sufficient to produce a sufficient amount of PA that qualifies as its ON state. We allow modifications from this assumption, but we require the enzyme and substrate of each reaction to appear as a group in the regulatory function of PA. A full list of constraints is indicated in S5 Text.

We used a set of 13 experimentally documented interactions among the existing nodes of the network as a pool, from which the algorithm can select edges to add to the model. The full list of edges in the pool is described in S5 Text. The algorithm added 8 edges from the pool (see the section entitled “New predictions” for more information).

The genetic algorithm improved both baseline models

It took roughly 17 hours to go through 100 iterations of the algorithm and generate 8099 models on a PC with an AMD Ryzen 5 3600 6-Core CPU at 3.8GHz. The majority of the computation time was spent on model evaluation; the evaluation of each model took roughly 7 seconds on average.

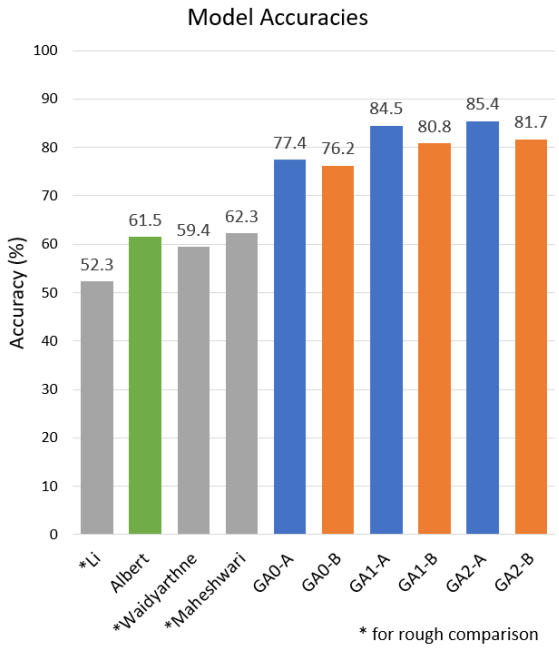

Model	Description
Li (2006)	39 nodes shared with the 2017 model
Albert (2017)	baseline A and B are made from this model
Waidyarathne (2018)	49 nodes shared with the 2017 model
Maheshwari (2019)	47 nodes shared with the 2017 model
GA0-A	no extra edges
GA0-B	no extra edges, alternate Ca^{2+}_c representation
GA1-A	main GA-refined model
GA1-B	alternate Ca^{2+}_c representation
GA2-A	more assumed edges, started from GA1-A
GA2-B	more assumed edges, started from GA1-B alternate Ca^{2+}_c representation

Figure 4. The accuracy of the previous ABA-induced stomatal closure models and the GA-refined models in reproducing a compilation of 505 perturbation experiments. The accuracy of the models marked with * is scaled to the percentage (50-75%) of experiments that apply to them. We note that 100% accuracy is not possible due to intrinsic limits on the agreement between the experiments on ABA-induced closure and Boolean models (see S6 Text). Detailed results are in the S5 Table.

We found that the genetic algorithm significantly improved both baseline models. The improved model A, which we will call GA1-A, achieved a score of 84.5%, significantly increased compared to its baseline of 61.7%. The improved model B, GA1-B, achieved a dramatic increase in score from 36.5% to 80.8%. To place these results into context, we present the accuracy of the previous manually constructed models as well as two additional versions of genetic algorithm-refined (GA-refined) models in Figure 4. In the GA0 models, we did not allow the addition of edges, therefore the GA0 models stay consistent with the original interaction graph. In contrast, for GA2 models (described in detail later) we allowed more assumed edges, without requiring experimental support. The figure indicates that all versions of GA-refined models surpass all published models, while at the same time decreasing the time needed for refinement from years to hours.

We evaluated the reproducibility of the genetic algorithm-based refinement by performing 8 independent GA1 runs starting from the baseline A model. The mean of the final scores was 81.2% with a standard deviation of 1.6%. The GA1-A model had the highest final score, 84.5%. There was a significant consensus among the GA1 model variants (e.g., 16 of the 35 functions that could change converged into an identical or logically equivalent form) as well as subtle dissimilarities that explain the differences in the score. The fitness score saturated before 100 iterations in each run. This shows that although the algorithm was not able to find the global maximum in every run, it was able to converge into a local maximum. This is a remarkable result considering the extremely high number of possible models for this case study. Indeed, we calculated using the Dedekind numbers that the lower bound of the number of Boolean models consistent with the interaction graph and the constraints is 10^{153}.

We indicate the regulatory functions of the GA1-A and GA1-B models in S7 Text. We evaluated the two models on the criteria of reversibility of closure, better accuracy, and recapitulation of the observed cases of closure in response to interventions.

Improvement 1. Reversibility

As 1 point in the score of a model means recapitulating the outcome of one experiment, the highest possible score for a genetic algorithm improved model is 505, the number of experiments in our compilation. The 2017 model recapitulated 314 experiments, out of which it received partial scores for 292 experiments. The reason behind the partial scores for the original model is the fact that its trap space repertoire in the absence of ABA includes a trap space with Closure=1 (as well as 16 trap spaces with Closure=0). For example, when the experimental observation corresponds to lack of closure (Closure=0) but the model result (i.e., the average value of the node Closure in the trap spaces) is nonzero, the model gets a partial score. The elimination of the trap space with Closure=1 would improve the model's score by 27.4 points. Importantly, the elimination of this trap space would simplify the dynamics by having a one-to-one correspondence between the signal ABA and the closure response, and as a consequence, it would also achieve reversibility.

Both GA1-A and GA1-B succeeded in achieving reversibility, thereby completely removing experiments that only gained a partial score due to the above reason (see Table 1). Note that they were not able to gain the maximum score improvement from reversibility due to trade-offs in capturing some of the experiments (i.e., due to the fact that achieving agreement with one experiment creates a disagreement with another experiment). It is particularly remarkable that this reversibility was achieved without the introduction of time-dependent regulatory functions as done in the 2020 revision [31].

Improvement 2. Better agreement with experimental results

The original model disagreed with 191 experiments. An improved model would need to preserve the original model's agreements with the experimental results and reach agreement with the experiments the original model did not capture. Indeed, the increase in score of both GA1-A and GA1-B compared to the original model is due to resolving the majority of the original model's discrepancies with experiments (see Table 1).

Table 1. Summary of the two sources of the improved score of the GA1-A and GA1-B models compared to the 2017 model [29]. The score gains (indicated in parentheses in the second column) of the genetic-algorithm-refined models arise from resolving 50% or more of the disagreements of the 2017 model with experimental results (third column) and eliminating multistability (fourth column). A small number of experiments were no longer captured by the revised models, decreasing the actual score gain (fifth column).

Model	Score (max 505)	Score gained from resolving original disagreements (max +167.1)	Score gained from reversibility (max +27.4)	Score change from new disagreements
2017	310.5 (61.5%)	-	-	-
GA1-A	426.9 (84.5%, +116.5)	+101.4	+25.3	-10.2
GA1-B	407.9 (80.8%, +97.4)	+85.9	+26.5	-14.9

Within the general goal of reaching better accuracy, we also checked the specific goal of reaching better agreement with the experimental interventions that cause closure in the absence of ABA. Table 2 summarizes the experimental observations and model results for the node Closure, with the interventions involving nodes studied by more experiments shown on the left. The categorization of the experimental results, ranging from Some (0.5) to ON (1), reflects the observed degree of closure (decrease of the stomatal aperture) induced by each intervention. The table also indicates the results of the 2017 model, the Maheshwari et al. 2019 model, and the two GA-refined models. The first observation is that according to our evaluation criteria (see Methods) the 2017 model agrees with the experimental results of four interventions (providing ROS, 8-nitro-cGMP, or InsP3, or inactivating AtRAC1). The 2019 follow-up to the model by Maheshwari et al. adds two more agreements (with providing CaIM and cADPR). GA1-A preserves the original model's agreements and has an improved score for the response to NO, pH_c, and PA. GA1-B preserves the agreement for three interventions, gets a lower score than the 2017 model in the case of supplying InsP3, and receives a higher score for CaIM, NO, and S1P. Note that the elements CaIM, NO, pH_c, and PA lie at the core of the system, as reflected in the large number of experiments studying them. It is particularly encouraging that the GA-refined models surpass both the 2017 and 2019 models in recapitulating interventions to these nodes. Overall, GA1-A reaches agreement with three more experimental observations compared to the 2017 model (out of six where improvement is possible), and GA1-B reaches agreement with two more experimental observations. We describe the mechanisms behind these results in the next sections.

Table 2. The experimental value of Closure in response to interventions in the absence of ABA and the corresponding predictions of four models. The interventions are listed in the decreasing order of the number of experiments that observed or manipulated the corresponding elements. The model entries indicate the categorization from lack of closure (0) to closure (1) described in the Methods. To aid the comparison of the models in recapitulating the experimentally observed closure responses, the entries are color-coded as black (agreement), dark red (partial agreement), or bright red (disagreement). The quantitative scoring of each result is indicated in S1 Table.

Intervention	ROS CA	CaIM CA	NO CA	pHc CA	PA CA	8ncGMP CA	cADPR CA	AtRAC1 KO	InsP3 CA	S1P CA
Experimental results	ON	ON	Some/ ON	Some/ ON	Some/ ON	Some	ON	Some/ ON	Some/ ON	Some/ ON
Albert 2017	1	0.5	0	0	0	0.5	0.5	0.5	0.5	0
Maheshwari 2019	1	1	0	0	0	-	1	1	1	0
GA 1-A	1	0.5	0.5	0.5	1	0.5	0.5	0.5	0.5	0
GA 1-B	1	1	0.5	0	0	0.5	0.5	0.5	0	0.5

Regulatory function revisions shared by the two GA-refined models

The two GA-refined models preserve the regulatory functions of 30 nodes; the remaining 28 regulatory functions were changed in one or both models. A significant fraction of the

modifications to regulatory functions are shared by both models (6 identical modifications and 13 very similar ones). We traced the effects of these modifications to the outcomes of the models and to the increase in their agreement with experimental results. We give a detailed description of these shared modifications in S8 Text. Five shared modifications use new edges from the experimentally supported pool, confirming the improvements possible from the incorporation of new biological information. A general trend in the shared modifications is the deletion of an assumed direct regulatory relationship that can also be explained by a logic chain (a succession of two or more relationships that has the same effect). In some of these cases, we could identify a shortcoming in the reasoning that led to the regulatory function in the original model. For example, including a regulator (in this case, ROS) as direct and necessary for a target node's activation (in this case, 8-nitro-cGMP) was less consistent with the totality of experimental evidence than having it as an indirect regulator, in which case it could be both necessary and sufficient. These findings illustrate how an automated method using a genetic algorithm can overcome modelers' bias in selecting edges and functions and can reveal the optimal possibilities.

The dynamics of the GA-refined models

Both GA1-A and GA1-B have a single minimal trap space (attractor) in the presence of ABA; these attractors recapitulate the experimental observations of the wild-type response to ABA and are similar to each other. The differences are in the nodes that oscillate in GA1-A due to the oscillations in Ca^{2+}_c and stabilize in their active state in GA1-B due to the activity of the Ca^{2+}osc node. Both GA-refined models have a single minimal trap space in the absence of ABA, in contrast to the original model, which has 17 minimal trap spaces. There is an almost perfect agreement between the minimal trap space of GA1-A and GA1-B. A significant agreement also exists between the minimal trap space of GA1-A and GA1-B in the case of ROS-induced stomatal closure.

In contrast, there is a significant difference between the minimal trap spaces in case of externally provided Ca^{2+}. We found that the 2017 model has two attractors. Both of these attractors exhibit oscillations in Ca^{2+}_c but they differ in the state of 33 nodes, including Closure. Only one of the attractors recapitulates the experimentally observed robust closure in response to external Ca^{2+} [46]. In contrast, each of GA1-A and GA1-B leads to a single attractor. The attractor of GA1-A features the oscillation of 47 nodes, including Closure. The attractor of GA1-B contains the ON state of the node Closure as well as of documented determinants of closure such as AnionEM. Considering the 6 elements whose status was measured under externally provided Ca^{2+} (pH_c, KEV, Microtubule depolymerization, Ca^{2+}_c, SLAC1, closure), GA1-A recapitulates 3 measurements and GA1-B recapitulates all 6, thus it is the best among the three models in terms of agreement with experiments.

There is a significant difference between minimal trap spaces in the case of providing NO in the absence of ABA as well. The two GA-refined models rely on different mechanisms to achieve agreement with the experimentally observed moderate closure. GA1-A has the same attractor as in the case of providing external Ca^{2+}; this attractor has many oscillating nodes, including Closure. GA1-B has two attractors; one has Ca^{2+}_cosc = Closure = 0 and the other has Ca^{2+}_cosc = Closure = 1. Considering the 5 elements whose status was assayed under externally provided NO (pH_c, ROS, 8-nitro-cGMP, PA, closure), GA1-A recapitulates four experiments, and GA1-B recapitulates all five.

In addition to tracing the genetic algorithm-induced modifications in the regulatory functions and the resulting dynamics to an improved agreement with the existing experimental

observations, it is also possible to extract novel predictions and suggest new experiments. In the following, we describe a selection of new predictions.

New predictions of the GA-refined models

Modifications to the interaction graph

Both GA-refined models feature significant changes to the interaction graph, which can serve as new predictions. GA1-A added 6 new edges from the pool and deleted 24 edges (of 152 starting edges). GA1-B added 7 new edges from the pool and deleted 17 edges (of 145 starting edges). The added edges present in both GA-refined models indicate biological mechanisms that were not included in the 2017 model. As shown in Table 3, five new edges were added in both models: Aquaporin→ ROS, ROS→ Actin reorganization, PA→ Microtubule depolymerization, PA-| ABI2, pH_c→Vacuolar acidification. Importantly, the added inhibitory edge between PA and ABI2 recapitulates the experimentally supported prediction of the 2019 follow-up to the 2017 model [30].

Table 3. Added edges in the GA-refined models compared to the original 2017 model [29]. Note that the inhibitory edge from PA to ABI2, which was incorporated in the 2019 revision of that model by Maheshwari et al. [30], was added by both GA-improved models.

	PA ⊣ ABI2	Aquaporin → ROS	ROS → AR	PA → MD	pH_c→VA	Other Edges
Maheshwari 2019	O	X	X	X	X	
GA 1-A	O	O	O	O	O	PA ⊣ HAB1
GA 1-B	O	O	O	O	O	$Ca^{2+}{}_c$osc ⊣ ABI2 AR → RBOH

AR: Actin Reorganization, MD: Microtubule Depolymerization, VA: Vacuolar Acidification

Ten edges were deleted in both models: $Ca^{2+}{}_c$→QUAC1, NO⊣KOUT, ROS→8-nitro-cGMP, ROS⊣H^+ ATPase, ROS⊣PP2CA, SCAB1→Actin Reorganization (omitted from Figure 5), SLAH3→AnionEM, and self loops on Vacuolar Acidification, MPK9/12 and Microtubule Depolymerization. A significant fraction of these edges represented assumptions of the 2017 model based on indirect evidence. These assumptions are no longer needed due to the improvements to the regulatory functions made possible by the genetic algorithm (see S8 Text for examples). Note that the deletion of an edge does not necessarily mean lack of influence; it indicates that in the context considered the influence is not significant enough to overcome the effects of the other regulators in a phenotypically relevant way.

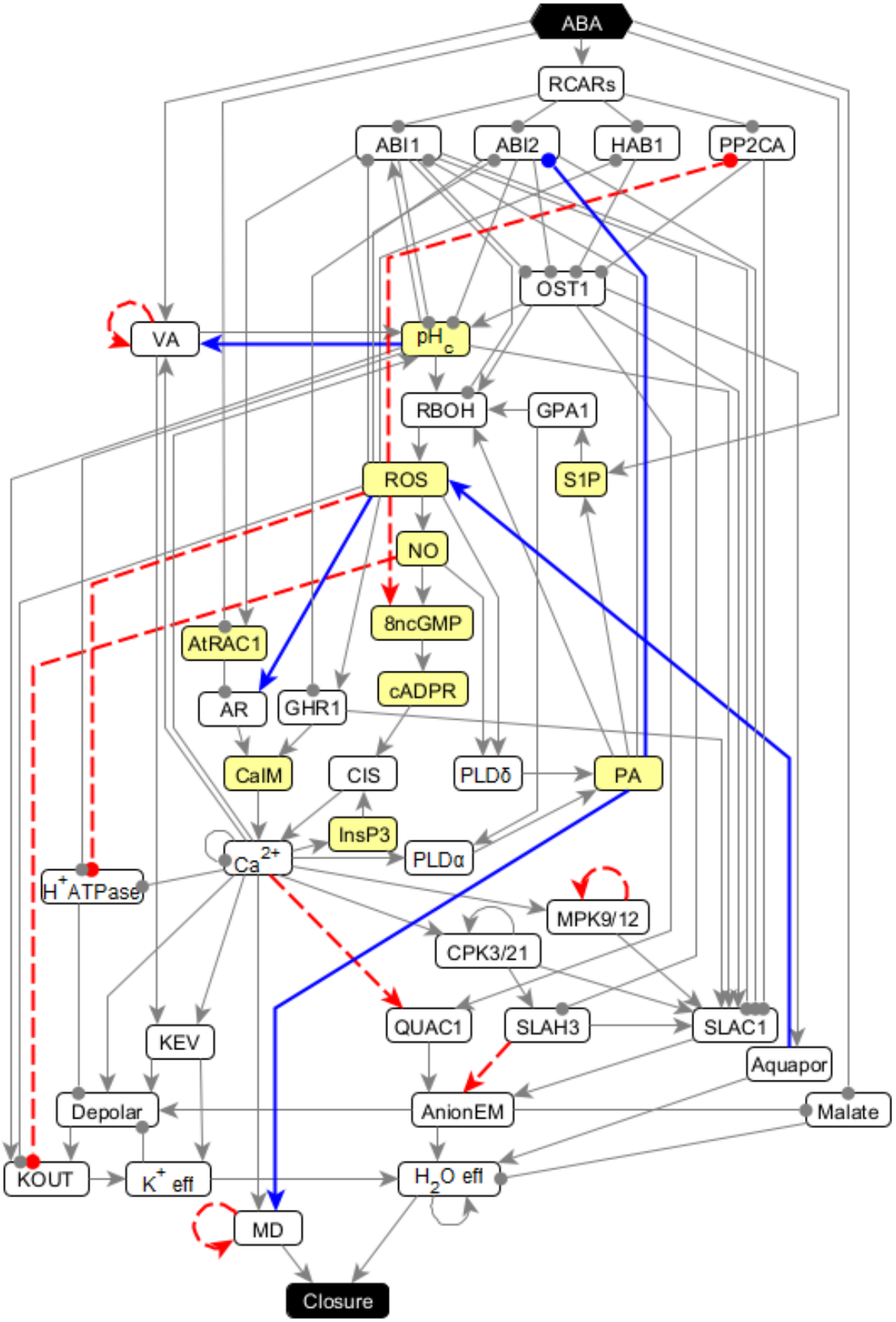

Figure 5. Simplified interaction graph illustrating the modifications to the network topology (edge deletions and additions) shared by the GA-refined models GA1-A and GA1-B. Each

edge that terminates in an arrowhead indicates a positive regulation, and a round tip means negative regulation. Blue edges are shared additions of the GA-refined models, and red dotted edges were deleted by both GA-refined models. The nodes with yellow background are the key intervention nodes whose constitutive activation (or inhibition in the case of AtRAC1) leads to some degree of Closure. The full names of the elements are indicated in S3 Table.

Predictions that can be verified experimentally

The GA-refined regulatory functions also serve as new biological predictions. We summarize selected testable predictions in Table 4 and explain them below.

One such prediction can be extracted from the shared modification to the regulatory function of OST1. Both GA-improved models recapitulate the experimentally observed inhibitory effect of ABI1 on QUAC1 by making ABI1 alone able to inhibit OST1 kinase activity. This results in the follow-up prediction that ABI1=1 leads to the insensitivity of Aquaporin to ABA; this prediction can be experimentally verified via methods used in [47].

The GA-refined models modify the regulatory function of SLAC1 such that it is easier to activate. As a consequence, they recapitulate the experimental observation that ROS activates SLAC1. A follow-up prediction is that the resulting anion flow brings the malate concentration below threshold.

Both GA-refined models modify the regulatory function of ROS by incorporating the documented role of aquaporins in bringing ROS into the cell. The necessity of this process for achieving a level of ROS sufficient to regulate its downstream targets implies that the disruption of aquaporins (in *pip2;1* KO mutants) will disrupt NO production, cADPR production (one of the sources of CIS), and the activation of PLDδ (one of the enzymes that catalyze PA production). Any impairment of NO production in *pip2;1* KO mutants in response to ABA or other closure-inducing signals can be experimentally tested using DAF2 fluorescence.

Yet another prediction is due to the shared features of the regulatory functions of PP2CA in the two models: PP2CA will be active in the absence of ABA or for knockout of the RCARs receptors even if ROS or other internal closure-inducing signal is provided. This prediction is testable by, e.g., assaying PP2CA phosphatase activity in response to ROS.

Causal relationships mediated by chains of interactions (pathways) can also yield new predictions. The 2017 model and the GA-refined models agree in predicting that ROS is sufficient to induce PA production. This is experimentally testable. As the GA-refined models incorporate the new observation that PA is sufficient for microtubule depolymerization, a follow-up testable prediction is that ROS can induce microtubule depolymerization; this can be tested by methods used in [48].

The shared features of the GA-refined models' attractors (e.g., the list of elements that are activated by any of multiple closure-inducing interventions) identify further predictions. The strong similarity of the GA models' attractors in response to providing NO, 8-nitro-cGMP, or cADPR suggests that the experimental observations of three elements (pH_c, ROS, PA) made in the case of providing NO can be extrapolated to the other interventions, for which no such assays were performed yet. Perhaps the most interesting of these observations is the lack of production of ROS under externally provided NO [49]. We find that the GA-refined models' minimal trap spaces in response to Ca^{2+} share this feature with the minimal trap spaces found in response to NO. This result leads to the prediction that external Ca^{2+} would yield no or a very limited amount of ROS production. While ROS

production in ABA-induced closure has been experimentally documented, the production of ROS in response to external Ca^{2+} has not yet been studied experimentally.

Table 4. Illustrative biological predictions that can be made based on the GA-refined models of ABA-induced closure.

Context	Prediction
Constitutive activation of ABI1 in the presence of ABA	The aquaporin channels will not activate (will not open)
Externally provided ROS in the absence of ABA	The malate concentration decreases below threshold.
	PA is produced
	The microtubules are depolymerized
Disruption of aquaporins (*pip2;1* KO) in the presence of ABA	Lack of NO production
	No cADPR production
	PLDδ is not activated
Externally provided ROS in the absence of ABA	PP2CA is active
Externally provided ROS, knockout of RCARs receptors, in the presence of ABA	PP2CA is active
Externally provided cADPR in the absence of ABA	pH_c increases to a lesser extent than in response to ABA
	No ROS production
	PA is produced
Externally provided 8-nitro-cGMP in the absence of ABA	pH_c increases to a lesser extent than in response to ABA
	No ROS production
	PA is produced
Externally provided Ca^{2+} in the absence of ABA	No ROS production

A more general insight can be gained from observing that GA1-A and GA1-B rely on two different mechanisms to yield minimal trap space results of 0.5 that achieve agreement with experimental observations classified as “Some” in Table 2. The attractors of GA1-A feature oscillations in Closure (as well as a significant number of other nodes), which are due to the oscillations of Ca^{2+}_c. In contrast, GA1-B has two attractors, one featuring Closure=1 and the other featuring Closure=0. Although different in a technical sense, these results are consistent with each other in that they both suggest population-level heterogeneity of the stomatal responses. Due to the challenges of tracking individual stomata in real time, there are few studies of individual stomata. Nevertheless, the studies that exist include observations of multiple types of oscillations in the stomatal aperture, including Ca^{2+}-induced oscillations (reviewed in [50]). In addition, [28] reported a significant bimodality of the ABA-treated stomatal aperture distribution. Our results suggest that more in-depth analyses of the time-dependent status of signaling mediators in individual guard cells may reveal a richer dynamic picture than previously thought.

Discussion

Small, local changes in a Boolean model, such as to the regulatory function of a single gene, can lead to global changes in the attractor repertoire and thus to the predicted phenotypes. This makes the process of iteratively building a model, or incorporating new biological knowledge into an existing model, extremely challenging. Here we automate the process of refining or updating an existing Boolean model. We use a genetic algorithm to adjust the regulatory functions of the model to improve its agreement with curated experimental results. Automated exploration and quantitative scoring of modeling decisions can alleviate the immense cognitive burden of integrating myriad experiments into a causal model while reducing human error and modeler bias. In contrast to competing Boolean approaches, our method uses a flexible scoring method that appropriately handles partial state data and the subtleties that arise in discretizing experimental data. In the case study considered here, for example, we used this flexibility to introduce additional outcome categories (e.g., “Some”, “OFF/Some”) to describe intermediate outcomes (e.g, reduced closure) and disagreement between experimental observations. Moreover, our workflow is the only viable automated approach in settings where full state data obtained from high-throughput measurements are not available. By considering the interdependence of perturbation experiments, our scoring achieves an unprecedented level of biological realism even with limited data.

Our method allows modelers to automatically explore many more modeling choices than previously possible, enabling systematic evaluation of alternate modeling assumptions (e.g. compressing an oscillating negative feedback loop into a single non-oscillating node, or introducing multiple levels of activation for a node). Such core modeling decisions can have large, global effects on the model dynamics, and hence switching to a different description of an important node’s regulatory logic often requires many adjustments to other nodes’ functions to reach an accuracy comparable to that of the original model. While it is difficult and time-consuming to manually evaluate and compare multiple core decisions, *boolmore* allows such adjustments to be made in a reasonable amount of time. As an illustrative example, we considered a model of ABA-induced closure in which the oscillating negative feedback between cytosolic calcium and calcium ATPase was replaced by a single node whose activity indicates calcium oscillation (baseline model B). Using *boolmore*, we refined baseline model B, which had an accuracy of only 36.5%, into model GA1-B, with an accuracy of 80.8%. Broad exploration of modeling choices can be further enhanced by workflow customization. Our workflow can be easily customized in multiple ways. The scoring system can be augmented by additional measures, such as the number of attractors, or the phenotype transitions under different environments, to produce more realistic models. Model prioritization can be customized so that only models with certain key behaviors are selected. Furthermore, the modeler has the freedom to determine how individual experimental results should be encoded; for instance, allowing for finer-grained response categories than used here.

Though *boolmore* worked well on models with randomized regulatory functions, it performs best when it starts from a pre-existing baseline model with reasonable regulatory functions. Starting with a high-quality interaction graph is especially important, as it can fundamentally constrain dynamical behaviors regardless of the Boolean functions. We found that a change in a single edge may lead to a great decrease in the agreement of the model with experimental results. When we corrected the 2017 model of ABA-induced stomatal closure by deleting the erroneous edge from Vacuolar acidification to KEV, *boolmore* could not refine the model to recapitulate ABA-induced closure without adding a new edge (a

self-edge on H_2O efflux) to compensate. Fortunately, many methods have been developed to construct or infer biomolecular interaction graphs [51,52], and curated interaction graphs are available in multiple databases [53–55], increasing the likelihood of a high-quality interaction graph for any cellular process to be modeled.

New discoveries that refine the interaction graph will improve the final fitness of the GA-refined model. We illustrate this trend by evaluating 3 versions of GA-refined models (see Figure 4 and S5 Table). The GA-refined models that did not allow edge addition (GA0-A and GA0-B) showed an overall 5.8% lower score than the GA1 models. We also considered GA-refined models that allowed 50% more additional edges than the 13 experimentally observed edges (GA2-A and GA2-B). We chose the assumed edges manually to help achieve agreement with top-of-the-hierarchy experiments. Two such edges were incorporated in the GA-improved models, both of which suggested new regulation of ion flows. For example, the suggested connection between CIS and anion flow allows the recapitulation of impaired anion flow in case of disruption of PLC or cADPR. The GA2-A and GA2-B models showed a 1.0% increase in scores on average, suggesting the existence of undiscovered interactions. This example shows that our workflow can be used to explore putative interactions whose incorporation can enhance model accuracy.

Although gaps of knowledge in the interaction graph can be filled by allowing the addition of edges, such addition is only effective in moderation; each additional edge doubles the size of the search space. Although *boolmore* can in principle search the whole space of Boolean functions consistent with the constraints, it can only search the local vicinity of the starting functions in the practical time limit. Model evaluation is the major computational bottleneck of *boolmore* and we believe that no trivial speedup is possible. By relying on the Python package *pyboolnet* [17], *boolmore* could find the minimal trap spaces in our 82-node case study in a hundredth of a second. Even with this remarkable speed, evaluating more than 8000 models under more than 260 perturbation settings resulted in 17 hours of runtime for a single run on a personal computer. Parallelization of the model evaluations may shorten the time required for each generation, and better-optimized parameters for the mutation and selection process may reduce the generations of models needed to reach saturation.

Any method that involves fitting to data has a chance of overfitting, i.e., inferring more parameters than can be justified by the data [56]. The parameters of a Boolean model are the Boolean functions of individual nodes. In our case study, *boolmore* deleted many edges that were included in the manually constructed starting models. Deletion of edges is analogous to removing parameters, and hence our workflow actually helped reduce the risk of overfitting that exists in the manual refinement process. Our workflow also helps introduce new edges in a much more conservative manner by only allowing edges that increase the accuracy of the model as a whole.The predictive power of the models refined by *boolmore* is evident in the benchmarks, where the refined models showed 95% accuracy over the validation set (which was not used in the refinement process).

There is an intrinsic limit to the degree to which a Boolean model can recapitulate quantitative experimental results (see S6 Text for specific examples in our case study). These limitations would be ameliorated by introducing multiple levels of activation for nodes. As the regulatory functions of multi-level nodes can be expressed as sets of Boolean functions [57], our binary representation can be expanded to accommodate multiple levels. A multi-level representation of the output variable “Closure” is especially needed in future models that integrate the response to the multiple signals that lead to various degrees of stomatal closure (ABA, high CO_2, darkness, and their combinations). *Boolmore* can be a

useful tool for exploring the possibilities for multi-level representations and finding those that agree with experiments the most.

To use our workflow, one needs a list of perturbation experiment results, as well as interactions and constraints coming from firm mechanistic knowledge. We highly recommend that every modeler gather and publish this data for each model, regardless of whether they intend to use our approach. Doing so provides a clear overview of the considered experiments and the modeler's interpretation of the results, allows for objective evaluation and comparison of different models of the same biological system, and facilitates follow-up research to expand or reinterpret the model.

Our automation of model refinement streamlines model-building by lowering the hurdle for the initial model. Once the experimental database and an interaction network for the model are set, a quickly achievable preliminary model can be refined in a fraction of the time that would be needed for manual model building. We envision that *boolmore* may also be used as an exploratory tool, allowing biologists and modelers to evaluate whether, and how, a model can accommodate hypothetical experimental results. *Boolmore* can also be integrated with other steps such as automated evidence gathering [58] and model expansion [59] to progress toward fully automated and extremely fast model construction.

Acknowledgements

We are grateful for the advice of Prof. István Albert, Prof. Sarah M. Assmann, Prof. Dezhe Jin, and the helpful suggestions of Dr. Xiao Gan, Dr. Fatemeh Sadat Fatemi Nasrollahi, and Eli Newby.

Data availability statement

Python package *boolmore* available at github repository https://github.com/kyuhyongpark/boolmore.

Supporting information

S1 Text. Key methodologies to identify the long-term behaviors of a Boolean system
S2 Text. Summary of prior work that used genetic algorithms for Boolean model inference or revision
S3 Text. Supplementary methods
S4 Text. Details of the interpretation of the "Some" category of experimental results
S5 Text. Details of the constraints, extra edges, and the starting models used for improving the ABA-induced closure model
S6 Text. Intrinsic limits on the agreement between experiments on ABA-induced closure and models
S7 Text. The Boolean functions of the 2017 model and of the two GA-improved models
S8 Text. Regulatory function revisions shared by the two GA-improved models

S1 Table. The scoring functions used in our workflow
S2 Table. Detailed benchmark results
S3 Table. The full name of the abbreviated node names in the ABA-induced closure models
S4 Table. Compilation of experimental results used to score the ABA-induced closure model
S5 Table. Summary of the scores and features of the genetic algorithm-modified models as compared to the original 2017 model of ABA-induced stomatal closure

Supporting information

S1 Text. Key methodologies to identify the long-term behaviors of a Boolean system

The state transition graph, made up by the 2^N states of the system and the possible transitions between them, provides a complete description of the model's dynamics, including the attractors and the states that lead to them. As the state transition graph is computationally expensive to calculate, modelers often choose to run simulations, which can be thought of as sampling trajectories (random walks) in the state transition graph. An effective alternative method to obtain a summarized state transition graph and determine the attractors of a Boolean model is via the identification of so-called stable motifs [7]. A stable motif is a self-sufficient feedback loop that can sustain an associated state of its constituent nodes regardless of the other nodes of the system. A conditionally stable motif (CSM) is a motif that acts like a stable motif as long as certain conditions are satisfied, for example, as long as a node external to the motif maintains a fixed state [9].

A subspace of a Boolean network is a subset of the state space characterized by a set of fixed node values, and a subspace is called a trap space if there are no dynamical trajectories that exit it. Once locked in, a stable motif is irreversible, and traps the system into a trap space [8]. A minimal trap space is a trap space that does not contain any smaller trap space within it. The successive locking-in of stable motifs and CSMs traps the system into smaller and smaller trap spaces, eventually reaching a minimal trap space [7,8]. A minimal trap space, or a quasiattractor, is a good approximation of an attractor. It is either a single state (a point attractor) or a set of states in which the nodes that are not fixed by stable motifs may oscillate between the 0 and 1 state. Calculating trap spaces is much faster than calculating attractors. In rare cases there may be multiple complex attractors in the same minimal trap space, or there may exist motif-avoidant attractors that lie outside of a trap space. These behaviors are dependent on the specifics of timing (update scheme) [8,60], and are unlikely in biological systems, which need to function robustly despite variations and stochasticity.

S2 Text. Summary of prior work that used genetic algorithms for Boolean model inference or revision

The most relevant prior work can be categorized based on the goal of the authors to infer a network together with a Boolean model, infer a Boolean model using a prior knowledge network, or revise/extend an existing Boolean model. We organize the key information about each algorithm in the table below. For each of the published algorithms we list the type of state input they require, whether or not they use a prior network, and describe a representative case study in which the algorithm was used.

Almost all algorithms (with the exception of Sayed et al) require system-wide input information, i.e., the knowledge of the state of all the nodes, in multiple conditions. When the number of conditions is of the same order of magnitude as the number of nodes, we refer to the state input as a "matrix". (Indeed, fewer conditions than the number of nodes make the model inference problem under-determined). Most studies assume that each state in the input reflects a point attractor (steady state). Four studies allow multi-state (oscillating) attractors as well, in which case we write "attractor".

Due to the different goals, the biological comparisons through which the output of the algorithm is evaluated also differ. If the goal is to infer a network together with a Boolean model, the accuracy of the output is mainly tested by evaluating the resulting edges. Most of

the existing algorithms for Boolean model inference (with Bonita being a notable exception) evaluate the model solely on its attractors. The two algorithms for model revision (RevMod and ARBoLoM) are solely tested on their ability to recapitulate the input (steady states or trajectories of the wild type system). It is important to note that these two algorithms are not set up to handle perturbation data. It is evident from the last column that almost all studies (with the exception of CellNetOptimizer) used artificial measurements to evaluate the algorithm.

Reference	State input	Prior network	Representative case study and result
Goal: Inference of an interaction network and Boolean model			
Trinh & Kwon[20]	Matrix of point attractor(s) of the WT system and for multiple perturbations	No prior network.	Artificial gene expression data generated from a 100 node network. More than 100 point attractors were used, including the point attractors of the WT system and the point attractor(s) in case of KO of each gene. The inferred network had a structural accuracy of ~95%; the regulatory functions were not evaluated.
Goal: Inference of a Boolean model			
Dorier et al. [21]	Matrix of point attractors of the system and the transitions between them in case of perturbations	The inferred network is a subset of a prior network.	Artificial measurements generated from a published 25-node Boolean model of cell fate decisions. The input consisted of 256 transitions between point attractors; the starting attractors are the four point attractors of the WT system and both KO and CA of each node are considered. The inferred model recapitulated the attractors obtained from individual KO of 14 key nodes.
Ghaffarizadeh et al. [22]	Attractors of the wild type system and for certain perturbations	If used, the prior network is fixed. The regulatory functions are assumed to be nested canalyzing functions.	Artificial expression profiles generated from a 11-node published Boolean model of myeloid cell differentiation. The edges of this model were used without information on their signs. The input contained four point attractors corresponding to four cell types and two constraints indicating the reduction in available cell types in case of KO of a certain gene. The inferred edge signs agree with prior literature on 26/30 edges.
Munoz et al (Griffin) [25]	The attractors of the wild type system, possibly expanded by attractors obtained in case of perturbations	The prior network can include hypothetical regulators and ambiguous effects	The network structure and set of 10 point attractors of a previously published 13-node Boolean model of *Arabidopsis thaliana* flower development are consistent with more than 300,000 Boolean models.
CellNOpt/CNO [36,61]	Matrix of point attractors of the wild type system under certain signals and perturbations	The prior network's edges can be pruned; new edges can be added one by one	Phospho-proteomics measurements of 16 proteins in response to one of 7 external molecules and for 7 cases of inhibition of a single protein. The prior knowledge network was reduced to include only the measured or inhibited nodes. The inferred model agreed well with experiments on combined inputs (to the

			same extent as with the input data).
Müssel et al. (CANTATA) [23]	Time series or attractors of the system	The prior network's edges can be pruned; new edges can be added randomly	Artificial measurements generated from a 10-node published Boolean model of the yeast cell cycle. The input consisted of the two most relevant point attractors and the most important sequence of 10 states. The actual network was modulated by 5 random changes. The inferred models reproduced the training set; the networks had a mean accuracy of ~98%.
Palli et al (Bonita) [24]	Matrix of states of the system under various conditions	The prior network is fixed. Each observed state is assumed to be a steady state (point attractor).	Artificial measurements generated from a 108-node KEGG pathway combined with biology-inspired random expression. Ninety percent of the inferred model's regulatory functions were equivalent to the functions used to generate the artificial measurements.
Goal: Extension or revision of an existing Boolean model			
Sayed et al [62]	The steady states of key nodes under various conditions	A group of new edges (each with one or two new nodes) are added to the prior network	A previously published 39-node Boolean model of T cell signaling was made incomplete by removing 8 nodes. An ensemble of candidate extensions that contained the removed nodes was analyzed. The input was obtained from the original model and consisted of the expression of five key nodes under two levels of an input signal. The inferred models restored at least four of the removed nodes and recapitulated the input.
Azpeitia et al [39]	The attractors of the wild type system	New edges are added to the prior network one by one. The new edges satisfy biological constraints.	After updating a previously published 10-node Boolean model of the gene regulatory network of the root stem cell niche with newly discovered interactions, it did not recapitulate two of the nine known attractors (all of which are point attractors) and had non-biological attractors. The application of the algorithm included 3 new interactions and yielded 10 very similar models that recapitulate all 9 attractors and have only 3 non-biological attractors each.
Gouveia et al. (RevMod)[37]	The point attractors of the wild type system	Edges of the prior network can be deleted or change sign. New edges can be added.	A previously published 40-node Boolean model of T cell receptor signaling was made incorrect by probabilistically changing regulatory functions, changing edge signs, removing or adding edges. The algorithm-revised model could recover the point attractors of the original model for the first three types of error, but timed out in most instances of added edges.
Aleixo et al (ARBoLoM)[38]	The point attractors or several trajectories of the wild type system	Edges of the prior network can be deleted or change sign. New edges can be added.	A previously published 40-node Boolean model of T cell receptor signaling was made incorrect by probabilistically changing regulatory functions, changing edge signs, removing or adding edges. The input consisted of the point attractors of the original model, or up to 5 trajectories with up to 20 timepoints. The algorithm-revised model could recover the

			correct point attractors or trajectories.

As Boolean models of biological systems are judged on their explanatory and predictive power in terms of the biological process they describe, the same standards should be used to evaluate inferred Boolean models as well. If a prior network is used, the accuracy of the model can be tested by evaluating its regulatory functions as well as its dynamical outcomes. If algorithm-driven additions to the prior network are allowed, these should be evaluated against the biological literature and may represent experimentally testable predictions. Such evaluation has not been a focus so far.

S3 Text. Supplementary methods

Detailed description of the model's outcome

In each comparison with the experimental result obtained in a perturbation condition, the model outcome is the average value of the observed node in the minimal trap spaces corresponding to that condition. If the node oscillates in a minimal trap space, we assign it the value 0.5. This value is used when averaging over multiple minimal trap spaces as well. For example, if there are two minimal trap spaces and the node oscillates in one and has the state 1 in the other, the average node value is 0.75.

The binary representation of regulatory functions

The interactions and regulatory relationships in biological networks are locally monotonic in the vast majority of cases. This means a regulator either inhibits or activates its target; it is not an inhibitor in one context (i.e., for a certain state of other regulators of the target node) and an activator in another context. The signs of the interactions are built from the literature, and form the foundation of the model. These interactions are often well established and hence changing the signs will lead to completely unrealistic networks.

To achieve random mutations of Boolean functions that preserve the original signs, we propose to represent the functions in a specific binary form. A positive update function (i.e., one for which all regulators are activators) with k inputs can be written in a disjunctive normal form

$$
\begin{aligned}
f(X_1,\ldots,X_k) = \\
& a_{\{\}} \mid \\
& a_{\{1\}}\&X_1 \mid \ldots \mid a_{\{k\}}\&X_k \mid \\
& a_{\{1,2\}}\&X_1\&X_2 \mid \ldots \mid a_{\{1,k\}}\&X_1\&X_k \mid \ldots \mid \\
& a_{\{2,3\}}\&X_2\&X_3 \mid \ldots \mid a_{\{2,k\}}\&X_2\&X_k \mid \ldots \mid \\
& \vdots \\
& a_{\{1,\ldots,k\}}\&X_1\&\ldots\&X_k
\end{aligned}
$$

Here **X** represents the vector composed of the state of the k input nodes, which includes X_0, X_1, X_2, … X_j, … X_{k-1}. The notation | means logical "OR" and & indicates logical "AND". A constant Boolean coefficient a_I is assigned to each subset I of input nodes, from I={} to I={1,...,k}. Note that this representation is not unique. The coefficients a_I can be ordered to obtain a binary representation of the function. A natural ordering interprets each I as the binary representation of the numbers from 0 to 2^k. This ordering is also traditionally used in the truth table representation of Boolean functions.

For example, let us consider three variables A, B, C and the function f(A,B,C) = B&C | A&B. This function can be written as f(A,B,C) = 0 | 0&C | 0&B | 1&B&C | 0&A | 0&A&C | 1&A&B | 0&A&B&C. Note that this representation includes all the possible subsets of ABC, leading to 2^3=8 clauses; the original three clauses are the terms that start with 1. The update function can be represented by a string of the a_i coefficients, i.e., f is represented by 00010010. The benefits of this representation are that any possible combination of 0s and 1s represents a positive function, and that the combinations span all the positive functions. Recall that this representation is not unique. For example, 00010011 also represents f because A&B&C is implied by B&C | A&B. However, the representation that has the maximal number of 1s (max representation) is unique and is equivalent to the truth table of the function (00010011 in this example). The representation that has the minimal number of 1s (min representation) is also unique and is equivalent to the Blake canonical form of the function (00010010 in this example).

This representation is mutated to get the mutated functions. For example, the mutation may change the sixth digit and lead to 00010110. The mutated function is thus f'(A,B,C) = 0 | 0&C | 0&B | 1&B&C | 0&A | 1&A&C | 1&A&B | 0&A&B&C, which can be further simplified to f'(A,B,C) = B&C | A&C | A&B.

This method can be extended to mutate locally monotonic functions that contain the NOT operator (which we will represent as !). If f(A,B) = !A&B, we can use the change of variables A' = !A and represent the function as the positive function f'(A,B)=A'&B. As long as we keep the original records of the signs, any locally monotonic function can be switched to a positive function, mutated, and switched back.

New edges can be added from a predetermined small pool of edges. For example, consider that node X, which had the original function f(A,B,C) = B&C | A&B | A&B&C, acquires a potential new positive regulator D. Its binary representation now has 16 digits instead of 8, thus acquiring 8 free parameters, which we mark with the symbol "?": f(A,B,C,D) = 0 | ?&D | 0&C | ?&C&D | 0&B | ?&B&D | 1&B&C | ?&B&C&D | 0&A | ?&A&D | 0&A&C | ?&A&C&D | 1&A&B | ?&A&B&D | 1&A&B&C | ?&B&C&D = 0?0?0?1?0?0?1?1?. If each "?" is set to zero, then the additional regulator is fully redundant, whereas the regulator is sufficient for activation if the first "?" is equal to one. When adding an additional regulator in *boolmore*, we initialize each "?" randomly, with a 50% chance to be 0 or 1.

The constraints of the regulatory functions are enforced by their binary representations. For example, if A is constrained to be a necessary regulator, any term that does not contain A will have a coefficient of 0 in the binary representation.

<u>Details of running the genetic algorithm</u>

The steps described in Figure 1 are performed on a population of 100 models in each iteration. We do 100 iterations in each run. The top 20 models with highest fitness scores from the previous iteration are carried over. Twenty pairs selected randomly (fitter models having a higher chance of being selected) from this top 20 are mixed pairwise to produce 20 new models. Finally, from this pool of 40 models, we repeat 60 times the process of selecting a model and mutating it, to generate the remaining 60 models of the new iteration. Fitter models have a higher chance of being selected in this process as well. Roughly 8000 networks were generated in a single run. These numbers were chosen such that the best score saturates by the end of the run in the benchmarks and the case study.

S4 Text. Details of the interpretation of the "Some" category of experimental results

We assigned the "Some" category to experimental observations that show an intermediate node activation level between the OFF state (which is determined based on the negative control) and the ON state (which is determined by the positive control). In our implementation, the model is considered to agree with the "Some" category if the average value of the node in the minimal trap spaces is near 0.5. This can be realized by an attractor in which the node oscillates, by multiple attractors with the node being with ON in some of the attractors and OFF in the other, or by a combination of oscillating and point attractors. However, there are multiple biological mechanisms that can yield such an intermediate activation level, and our scoring method can be customized to reflect them if they are known.

Most observations on the activation of cellular elements are population-averaged, which also yields an implicit time-averaging when the cells in the population are not synchronized. Hence, the biology underlying an observed intermediate activation level can belong to one of 3 broad categories. First, it could happen that the element's activation level oscillates in each cell, but the population-average shows an intermediate value. An example of such oscillation in our case study is the transient spikes of cytosolic calcium level in stomatal guard cells. Such oscillation can be verified when time-course observations of single cells are available [42]. Second, the population can be bimodal, with the element being ON in some cells and being OFF in the others. This behavior can be verified when the distribution of the individual cell activation level is available. Last, it could happen that the activation level is indeed intermediate in every individual cell over time.

If there is evidence for oscillation or bimodal distribution, our workflow can be customized to give a score only when the generated models reflect the actual dynamics. In our case study this was unnecessary as the calcium oscillation was guaranteed by the network structure. A Boolean model has no simple way of reflecting the last case, when the activation level is actually intermediate. One possibility, used in previous modeling [63], is to interpret oscillations of the Boolean model as excursions (repeated increases and decreases) around a dynamic equilibrium, and equate the fraction of the ON state with the observed intermediate level. The other possibility is to introduce an intermediate activation level, either by making the model multi-level, or by introducing a new node, which represents the intermediate activation level, into the Boolean model.

S5 Text. Details of the constraints, extra edges, and the starting models used for improving the ABA-induced closure model

<u>List of constraints</u>

1. fixed functions: Ca^{2+} ATPase, Ca^{2+}_c (Ca^{2+}_c osc), Closure, DAG, H_2O efflux, InsP3, InsP6, NO, PtdIns(3,5)P2, PtdIns(4,5)P2, RCARs, cADPR, cGMP
2. edge preservation: RCARs ⊣ ABI1, RCARs ⊣ ABI2, RCARs ⊣ HAB1, RCARs ⊣ PP2CA, KEV→K^+ efflux, KOUT→K^+ efflux, ABI1 ⊣ OST1, ABI2 ⊣ OST1, AnionEM→Depolarization
3. preservation of "necessary" logic: cGMP→8-nitro-cGMP, Depolarization→KOUT, PEPC→Malate, AnionEM ⊣ Malate, NADPH→ROS, RBOH→ROS
4. grouped regulation: (PC, PLDα),(PC, PLDδ),(DAG, DAGK)→PA, (SPHK1/2, Sph)→S1P/PhytoS1P
5. possible source: GEF1/4/10

List of the pool of extra edges and their experimental support

1. Ca2c ⊣ ABI2, HAB1, PP2CA, PA ⊣ ABI2, HAB1, PP2CA
These edges originate from the experimental observation that Ca^{2+} inhibits the phosphatase activity of PP2C family members [30].
Also, according to [64] PA binds to and inhibits PP2CA; 40% of the phosphatase activity of PP2CA is lost for 100 μM PA.

2. Aquaporin(PIP2;1) → ROS
As described in [65], RBOHs produce extracellular superoxide by transferring electrons from NADPH or FADH2 to oxygen. This extracellular H_2O_2 enters the plant cells through plasma membrane aquaporins. Reference [66] shows that knocking out Aquaporin eliminated ROS production under ABA.

3. Actin Reorganization → RBOH
Reference [67] showed that alteration of actin reorganization delays ABA-evoked H_2O_2 generation in guard cells. This effect of actin reorganization can explain a previously observed indirect effect of PtdInsP3 and PtdInsP4 (both regulators of actin reorganization) on ABA-induced ROS production [68,69].

4. ROS → Actin Reorganization
Reference [67] found that actin reorganization was impaired in *atrbohd/f* mutants (which lack RBOH), and that exogenous H_2O_2 application to *atrbohd/f* mutant leaves induced actin reorganization.

5. PA → Microtubule Depolymerization
In the 2017 model Microtubule Depolymerization is activated by TCTP, which in turn is regulated by Ca^{2+}_c. Figure 4f of [70] indicates that PA leads to microtubule depolymerization even in the absence of Ca^{2+}_c, suggesting the existence of a Ca^{2+}-independent mechanism.

6. pH_c → Vacuolar Acidification
Reference [71] suggests a positive feedback loop in which vacuolar acidification positively affects pH_c (and is necessary for it) and pH_c positively affects vacuolar acidification (and is necessary for it). The first part is incorporated in the 2017 model whereas the second part is not in the model.

7. ABI1 → GEF1/4/10
GEF1/4/10, considered a source node in the 2017 model, was found to be regulated by ABI1 [45]. ABA leads to the degradation of GEF1, likely promoted by CPKs [72]. ABI1 protects GEF1 from degradation.

8. GHR1 → CPK3/21
GHR1 is found to interact with CPK3 [73], probably acting as a scaffold to bring CPK3 to SLAC1.

Description of the baseline models

The 2017 model had an erroneous edge between the node Vacuolar Acidification and the node KEV, which represents vacuolar K^+ channels; this was recognized in a later publication

[43]. We found that the model corrected by deleting this edge had low accuracy, with a score of 291.7/505 (57.8%), and in response to ABA it exhibited oscillating stomatal closure driven by Ca^{2+}_c oscillations. To have a starting model that recapitulates the core behavior of ABA-induced closure, we pursued two avenues of correction of different scope.

First, drawing inspiration from the original model, which assumed self-sustained activity of four nodes that would otherwise exhibit Ca^{2+}_c-driven oscillations, we sought to identify a node between KEV and the output node Closure for which a self-sustaining influence would be biologically justified and able to yield sustained closure. After considering multiple nodes, we chose the abstract process node "H_2O efflux", whose inputs include AnionEM, K^+ efflux, Malate, and Aquaporin. Indeed, sustained water efflux from the guard cells through the aquaporin channels is a hallmark of stomatal closure. The improved regulatory function expresses the assumption that water efflux, once started, can be sustained even if K^+ efflux stops, if all other conditions continue to be met. The original model with the corrected KEV function and improved H_2O efflux function recapitulated ABA-induced closure and had a score of 311.7/505 (61.7%). We adopted this model as the first baseline model (A).

Our second correction introduced a global, qualitative change to the model by implementing a different representation of the dynamics of cytosolic Ca^{2+}. We replaced the two-node negative feedback loop with a single node, 'Ca^{2+}_c osc', whose ON state represents the appearance of Ca^{2+} elevation transients and whose OFF state represents an unchanged cytosolic Ca^{2+} level. This node is an equivalent representation of the Ca^{2+}_c oscillation in the 2017 model. As a further implementation of the change, we replaced "Ca^{2+}_c" by "Ca^{2+}_c osc" for every target of Ca^{2+}_c, and we deleted the four self-edges. The replacement of an oscillating node with a non-oscillating one is a potentially dramatic change, because it stabilizes the positive regulation and positive feedback loops in the system. We found that the thus-modified model had a score of only 184.2/505 (36.5%), mainly because it did not recapitulate the reduction of ABA-induced closure for single-node interventions. We adopted this model as our second baseline (B), aiming to find out whether the genetic algorithm is able to improve it to an accuracy that surpasses the 2017 model's.

S6 Text. Intrinsic limits on the agreement between experiments on ABA-induced closure and models

We analyzed the discrepancies between experimental observations and the results of GA-refined models and identified several types of causes. The first type is made up of inconsistencies between experimental results that cannot be resolved by any model. The second type represents quantitative effects that cannot be reflected by a Boolean model. The third type has to do with the limitations imposed by the interaction network.

<u>Inconsistencies between experimental results:</u>

The molecules DAG and InsP3 are the two products of the PLC-catalyzed hydrolysis of PtdIns(4,5)P2. As they are produced by the same reaction, their level should be the same. There is no improvement to the model that can recapitulate both the observation of ABA-induced InsP3 production [74] and the observation of no/very little DAG in the presence of ABA [75].

The pair of observations that (i) depletion of ROS impairs ABA-induced closure [49] and (ii) *gpa1* KO plants do not produce ROS in response to ABA [76], is not compatible with the observation that GPA1 KO leads to wild type ABA-induced closure [77].

Quantitative effects that cannot be reflected by a Boolean model:

The Boolean representation of an enzyme-catalyzed reaction requires the activity of the enzyme for the reaction to proceed and yield product. The experimental observation that providing nitrite (the reactant of the reaction that yields NO) leads to stomatal closure [78] cannot be captured in this framework. The likely resolution of the discrepancy is that a non-physiologically large amount of nitrite was provided.

CIS and CaIM are the two mechanisms of increase in the cytosolic Ca^{2+} level. Any Boolean function would assign a symmetrical influence to them (either both are sufficient, or both are necessary). In contrast, experimental results suggest an unequal contribution of CIS and CaIM [79].

The model characterizes the physiological processes that determine stomatal closure (e.g. K^+ efflux, H_2O efflux, Microtubule depolymerization) as necessary regulators of closure, whose disruption leads to Closure=0. Experimental results in which disruption of one of these processes led to reduced (but not absent) ABA-induced closure [70] cannot be recapitulated by the model.

Limitations imposed by the interaction network:

If the network contains a linear pathway A→B→C, the results of activating A, B, or C should be the same, as are the results of inhibiting A, B, or C. There were cases in which the perturbation of two nodes that participate in a linear pathway did not yield the same experimental result. For example, providing 8-nitro-cGMP led to a qualitatively smaller degree of closure than providing cADPR, which cannot be captured by the model's 8-nitro-cGMP→ADPRc→cADPR linear pathway. The differences may be due to quantitative effects or to missing edges.

"Actin reorganization" is a node that represents a two-step process: the disassembly and turnover of actin filaments, then their reassembly in a different configuration. The protein SCAB1 bundles and stabilizes actin filaments. The experimental observations that either knockout of SCAB1 or overexpression of SCAB1 delays actin reorganization [80] can only be captured if the two steps of the process are represented by separate nodes.

S7 Text. The Boolean functions of the 2017 model and of the two GA-improved models

In these functions the state variable of each node is represented by the name of the node, and the future state of each node is denoted by using an asterisk. For example C* = A or B means that the state of node C will be updated to 1 when A=1 or B=1. The functions reflect the notation used in the code of our algorithm; certain node names are written slightly differently in the code compared to the manuscript to avoid running errors. The full name of each node can be found in the S3 Table. The logical operator & indicates AND, | indicates OR and ! indicates NOT.

Boolean functions of the 2017 model:

8-nitro-cGMP* = NO & ROS & cGMP
ABA* = ABA
ABH1* = 1
ABI1* = !PA & ROP11 & !ROS & pHc | !PA & !RCARs & !ROS & pHc
ABI2* = ROP11 & !ROS | !RCARs & !ROS
ADPRc* = 8-nitro-cGMP
ARP_Complex* = 1
Actin_Reorganization* = ARP_Complex & !AtRAC1 & PtdInsP4 & SCAB1 | ARP_Complex & !AtRAC1 & PtdInsP3 & SCAB1
AnionEM* = QUAC1 & SLAH3 | SLAC1
AquaporinPIP2_1* = OST1
AtRAC1* = ABI1 | !ABA
CIS* = cADPR | InsP6 | InsP3
CPK23* = 1
CPK3_21* = Ca2c | CPK3_21
CPK6* = 1
Ca2_ATPase* = Ca2c
Ca2c* = !Ca2_ATPase & CaIM | CIS & !Ca2_ATPase
CaIM* = GHR1 & MRP5 & NtSyp121 | SACC | !ERA1 | !ABH1
Closure* = H2O_Efflux & Microtubule_Depolymerization
DAG* = PLC & PtdIns4_5P2
DAGK* = 1
Depolarization* = KEV & !K_efflux | !H_ATPase & KEV | Ca2c & !K_efflux | Ca2c & !H_ATPase | AnionEM & !K_efflux | AnionEM & !H_ATPase
ERA1* = 1
GAPC1_2* = 1
GCR1* = 1
GEF1_4_10* = 0
GHR1* = !ABI2 & ROS
GPA1* = S1P_PhytoS1P | !GCR1
GTP* = 1
H2O_Efflux* = AnionEM & AquaporinPIP2_1 & K_efflux & !Malate
HAB1* = !RCARs & !ROS
H_ATPase* = !Ca2c & !ROS & !pHc
InsP3* = PLC & PtdIns4_5P2
InsP6* = InsP3
KEV* = Vacuolar_Acidification | Ca2c
KOUT* = Depolarization & pHc | Depolarization & !ROS | Depolarization & !NO
K_efflux* = KEV & KOUT
MPK9_12* = MPK9_12 | Ca2c
MRP5* = 1
Malate* = !ABA & !AnionEM & PEPC
Microtubule_Depolymerization* = TCTP | Microtubule_Depolymerization
NAD* = 1
NADPH* = 1
NIA1_2* = ROS
NO* = NADPH & NIA1_2 & Nitrite
NOGC1* = NO
Nitrite* = 1
NtSyp121* = 1
OST1* = !HAB1 & !PP2CA | !ABI2 & !PP2CA | !ABI2 & !HAB1 | !ABI1 & !PP2CA | !ABI1 & !HAB1 | !ABI1 & !ABI2

PA* = PC & PLDdelta | PC & PLDalpha | DAG & DAGK
PC* = 1
PEPC* = !ABA
PI3P5K* = ABA
PLC* = Ca2c
PLDalpha* = Ca2c & GPA1
PLDdelta* = GAPC1_2 & ROS | NO
PP2CA* = !RCARs & !ROS
PtdIns3_5P2* = PI3P5K
PtdIns4_5P2* = PtdInsP4
PtdInsP3* = 1
PtdInsP4* = 1
QUAC1* = Ca2c & OST1
RBOH* = !ABI1 & GPA1 & OST1 & PA & PtdInsP3 & RCN1 & pHc
RCARs* = ABA
RCN1* = 1
ROP11* = GEF1_4_10
ROS* = NADPH & RBOH
S1P_PhytoS1P* = SPHK1_2 & !SPP1 & Sph
SACC* = Actin_Reorganization
SCAB1* = 1
SLAC1* = !ABI1 & !ABI2 & CPK6 & GHR1 & MPK9_12 & OST1 & !PP2CA & pHc | !ABI1 & !ABI2 & CPK3_21 & GHR1 & MPK9_12 & OST1 & !PP2CA & pHc | !ABI1 & !ABI2 & CPK23 & GHR1 & MPK9_12 & OST1 & !PP2CA & pHc
SLAH3* = !ABI1 & CPK3_21 & CPK6 | !ABI1 & CPK23 & CPK3_21
SPHK1_2* = PA | ABA
SPP1* = 0
Sph* = 1
TCTP* = Ca2c
V-ATPase* = Ca2c
V-PPase* = PtdIns3_5P2
Vacuolar_Acidification* = Vacuolar_Acidification | V-PPase | V-ATPase
cADPR* = ADPRc & NAD
cGMP* = GTP & NOGC1
pHc* = !ABI1 & !ABI2 & OST1 & Vacuolar_Acidification | Ca2c & Vacuolar_Acidification

Boolean function of the GA1-A model:
8-nitro-cGMP* = NO & cGMP
ABA* = ABA
ABH1* = 1
ABI1* = !PA & !RCARs | !PA & !ROS & pHc | ROP11 & pHc
ABI2* = !RCARs & ROP11 | !PA
ADPRc* = 8-nitro-cGMP
ARP_Complex* = 1
Actin_Reorganization* = ARP_Complex & !AtRAC1 & PtdInsP3 & PtdInsP4 | ARP_Complex & !AtRAC1 & PtdInsP3 & ROS | PtdInsP3 & PtdInsP4 & ROS
AnionEM* = QUAC1 & SLAC1
AquaporinPIP2_1* = OST1
AtRAC1* = ABI1 | !ABA
CIS* = InsP3 | cADPR
CPK23* = 1
CPK3_21* = CPK3_21 & Ca2c

CPK6* = 1
Ca2_ATPase* = Ca2c
Ca2c* = !Ca2_ATPase & CaIM | CIS & !Ca2_ATPase
CaIM* = !ABH1 & SACC | GHR1 | MRP5 & NtSyp121 & SACC
Closure* = H2O_Efflux & Microtubule_Depolymerization
DAG* = PLC & PtdIns4_5P2
DAGK* = 1
Depolarization* = AnionEM & !H_ATPase | Ca2c & !H_ATPase | !H_ATPase & KEV
ERA1* = 1
GAPC1_2* = 1
GCR1* = 1
GEF1_4_10* = 0
GHR1* = !ABI2
GPA1* = S1P_PhytoS1P | !GCR1
GTP* = 1
H2O_Efflux* = AnionEM & AquaporinPIP2_1 & K_efflux & !Malate | AnionEM & AquaporinPIP2_1 & H2O_Efflux & !Malate
HAB1* = !RCARs & !PA | !ROS & !PA
H_ATPase* = !pHc
InsP3* = PLC & PtdIns4_5P2
InsP6* = InsP3
KEV* = Ca2c
KOUT* = Depolarization
K_efflux* = KEV & KOUT
MPK9_12* = Ca2c
MRP5* = 1
Malate* = !ABA & !AnionEM & PEPC
Microtubule_Depolymerization* = PA
NAD* = 1
NADPH* = 1
NIA1_2* = ROS
NO* = NADPH & NIA1_2 & Nitrite
NOGC1* = NO
Nitrite* = 1
NtSyp121* = 1
OST1* = !ABI1 & !ABI2 | !ABI1 & !HAB1
PA* = DAG & DAGK & PC & PLDalpha | PC & PLDdelta
PC* = 1
PEPC* = !ABA
PI3P5K* = ABA
PLC* = Ca2c
PLDalpha* = Ca2c
PLDdelta* = GAPC1_2 & NO & ROS
PP2CA* = !RCARs
PtdIns3_5P2* = PI3P5K
PtdIns4_5P2* = PtdInsP4
PtdInsP3* = 1
PtdInsP4* = 1
QUAC1* = OST1
RBOH* = GPA1 & OST1 & PA & PtdInsP3 & RCN1 & pHc
RCARs* = ABA
RCN1* = 1

ROP11* = GEF1_4_10
ROS* = NADPH & RBOH & AquaporinPIP2_1
S1P_PhytoS1P* = SPHK1_2 & Sph
SACC* = Actin_Reorganization
SCAB1* = 1
SLAC1* = !ABI1 & !ABI2 & CPK23 & CPK6 & GHR1 & MPK9_12 | !ABI1 & !ABI2 & CPK23 & GHR1 & MPK9_12 & OST1 | !ABI1 & !ABI2 & CPK6 & GHR1 & OST1 | !ABI2 & CPK23 & CPK3_21 & GHR1 & OST1 & pHc | !ABI2 & CPK23 & GHR1 & MPK9_12 & pHc | !ABI2 & CPK6 & GHR1 & OST1 & !PP2CA & pHc
SLAH3* = CPK23 & CPK3_21 | CPK3_21 & CPK6
SPHK1_2* = PA | ABA
SPP1* = 0
Sph* = 1
TCTP* = Ca2c
V-ATPase* = Ca2c
V-PPase* = PtdIns3_5P2
Vacuolar_Acidification* = V-ATPase | V-PPase & pHc
cADPR* = ADPRc & NAD
cGMP* = GTP & NOGC1
pHc* = !ABI1 & OST1 & Vacuolar_Acidification | !ABI2 & Ca2c | Ca2c & OST1

Boolean functions of the GA1-B model:
8-nitro-cGMP* = NO & cGMP
ABA* = ABA
ABH1* = 1
ABI1* = !PA & !ROS | !RCARs & ROP11 & !ROS & pHc
ABI2* = !RCARs & !Ca2osc & !PA | ROP11 & !Ca2osc | !ROS & !Ca2osc
ADPRc* = 8-nitro-cGMP
ARP_Complex* = 1
Actin_Reorganization* = ARP_Complex & !AtRAC1 & PtdInsP3 & PtdInsP4 & ROS
AnionEM* = QUAC1 & SLAC1
AquaporinPIP2_1* = OST1
AtRAC1* = ABI1 | !ABA
CIS* = InsP6 & cADPR
CPK23* = 1
CPK3_21* = Ca2osc
CPK6* = 1
Ca2osc* = CaIM | CIS
CaIM* = !ABH1 & !ERA1 & GHR1 & MRP5 | !ABH1 & MRP5 & SACC | !ERA1 & GHR1 & NtSyp121 | !ERA1 & MRP5 & SACC | GHR1 & MRP5 & NtSyp121
Closure* = H2O_Efflux & Microtubule_Depolymerization
DAG* = PLC & PtdIns4_5P2
DAGK* = 1
Depolarization* = AnionEM & !H_ATPase | AnionEM & !K_efflux
ERA1* = 1
GAPC1_2* = 1
GCR1* = 1
GEF1_4_10* = 0
GHR1* = !ABI2 & ROS
GPA1* = S1P_PhytoS1P
GTP* = 1
H2O_Efflux* = AnionEM & AquaporinPIP2_1 & K_efflux & !Malate

HAB1* = !RCARs | !ROS
H_ATPase* = !Ca2osc
InsP3* = PLC & PtdIns4_5P2
InsP6* = InsP3
KEV* = Ca2osc
KOUT* = Depolarization & !ROS | Depolarization & pHc
K_efflux* = KEV & KOUT
MPK9_12* = Ca2osc
MRP5* = 1
Malate* = !ABA & !AnionEM & PEPC
Microtubule_Depolymerization* = TCTP | PA
NAD* = 1
NADPH* = 1
NIA1_2* = ROS
NO* = NADPH & NIA1_2 & Nitrite
NOGC1* = NO
Nitrite* = 1
NtSyp121* = 1
OST1* = !ABI1 & !ABI2 | !ABI1 & !PP2CA | !HAB1
PA* = PC & PLDdelta | PC & PLDalpha | DAG & DAGK
PC* = 1
PEPC* = !ABA
PI3P5K* = ABA
PLC* = Ca2osc
PLDalpha* = GPA1
PLDdelta* = GAPC1_2 & NO & ROS
PP2CA* = !RCARs
PtdIns3_5P2* = PI3P5K
PtdIns4_5P2* = PtdInsP4
PtdInsP3* = 1
PtdInsP4* = 1
QUAC1* = OST1
RBOH* = !ABI1 & GPA1 & OST1 & PtdInsP3 & RCN1 & pHc | !ABI1 & OST1 & Actin_Reorganization | GPA1 & OST1 & Actin_Reorganization | OST1 & PA & Actin_Reorganization | PA & PtdInsP3 & RCN1 & Actin_Reorganization | RCN1 & pHc & Actin_Reorganization
RCARs* = ABA
RCN1* = 1
ROP11* = GEF1_4_10
ROS* = NADPH & RBOH & AquaporinPIP2_1
S1P_PhytoS1P* = SPHK1_2 & Sph
SACC* = Actin_Reorganization
SCAB1* = 1
SLAC1* = !ABI1 & !ABI2 & CPK23 & CPK6 & MPK9_12 & pHc | !ABI1 & !ABI2 & CPK3_21 & CPK6 & MPK9_12 & !PP2CA & pHc | !ABI1 & !ABI2 & CPK3_21 & GHR1 & MPK9_12 & pHc | !ABI2 & CPK3_21 & MPK9_12 & OST1 & pHc
SLAH3* = !ABI1 & CPK23 & CPK3_21
SPHK1_2* = ABA
SPP1* = 0
Sph* = 1
TCTP* = Ca2osc
V-ATPase* = Ca2osc
V-PPase* = PtdIns3_5P2

Vacuolar_Acidification* = V-ATPase | V-PPase | pHc
cADPR* = ADPRc & NAD
cGMP* = GTP & NOGC1
pHc* = !ABI1 & OST1 & Vacuolar_Acidification | Ca2osc & OST1 | Ca2osc & Vacuolar_Acidification

S8 Text. Regulatory function revisions shared by the two GA-improved models

The two genetic-algorithm-improved models contain 6 identical modifications and 13 very similar ones out of 58 total regulatory functions. In the following we describe 10 shared modifications, their support in the experimental literature, and the insights they provide.

ROS* = Aquaporin(PIP2;1) & RBOH
Original: ROS* = RBOH
Both models adopt the experimentally supported Aquaporin(PIP2;1)→ ROS edge [65,66] from the pool.

Microtubule Depolymerization* = PA (GA1-A)
Microtubule Depolymerization* = PA | TCTP (GA1-B)
Original: Microtubule Depolymerization* = TCTP | Microtubule Depolymerization
Both models adopt the experimental-evidence-supported edge from PA to Microtubule depolymerization [64,70] from the pool as a sufficient mechanism. Specifically, [70] indicates that PA leads to microtubule depolymerization even when the cytosolic Ca^{2+} level is clamped (which would abolish the activation of TCTP, the other regulator of the node Microtubule Depolymerization).

ABI2* = !PA (GA1-A)
ABI2* = !Ca^{2+}osc & !PA & !RCARs | !Ca^{2+}osc & !ROS (GA1-B)
Original: ABI2* = !RCARs & !ROS
Both models adopt an indirect (GA1-A) or both direct and indirect (GA1-B) inhibitory effect from Ca^{2+}_c to ABI2, recapitulating the experimental results and prediction from Maheshwari et al. [30]. GA1-A couples this with the loss of the two original inhibitors. This loss does not significantly affect the settings under which ABI2 is activated, as PA is activated by ABA or ROS.

Vacuolar Acidification* = V-PPase & pH_c | V-ATPase (GA1-A)
Vacuolar Acidification* = pH_c | V-PPase | V-ATPase (GA1-B)
Original: Vacuolar Acidification* = Vacuolar Acidification | V-PPase | V-ATPase
Interpretation: The 2017 model included two vacuolar proton pumps (the V-ATPase and the V-PPase) as independent activators of vacuolar acidification. As experimental evidence indicates the existence of a positive feedback loop between the cytosolic and vacuolar pH level [71], we included an edge from pH_c to Vacuolar acidification to the pool. Both models incorporate this edge; both also omit the assumption of self-sustained activity in the 2017 model. The coupling of the effect of pH_c and V-PPase is different in the two functions.

Actin Reorganization* = ARP Complex & !AtRAC1 & PtdInsP3 & PtdInsP4 | ARP Complex & !AtRAC1 & PtdInsP3 & ROS | PtdInsP3 & PtdInsP4 & ROS (GA1-A)
Actin Reorganization* = ARP Complex & !AtRAC1 & PtdInsP3 & PtdInsP4 & ROS (GA1-B)

Original: Actin Reorganization* = (PtdInsP4 | PtdInsP3) & ! AtRAC1 & ARP Complex & SCAB1
Both GA1-A and GA1-B add ROS as a regulator of actin reorganization, but ROS combines with !AtRAC1 with “OR” in GA1-A and with “AND” in GA1-B. This means that actin reorganization can happen in response to ROS in GA1-A but only in response to ABA in GA1-B. In addition, the effect of SCAB1 on Actin reorganization is lost in both models. This is probably due to the fact that both SCAB1 KO and SCAB1 overexpression only delay actin reorganization [80] .

8-nitro-cGMP* = NO & cGMP
Original: 8-nitro-cGMP* = NO & ROS & cGMP
The published model incorporated the evidence that providing NO or ROS leads to the production of 8-nitro-cGMP, and ROS KO inhibits ABA-induced production of 8-nitro-CGMP [81], by assuming that both ROS and NO are direct and necessary regulators of 8-nitro-cGMP (in addition to its substrate, cGMP). The GA-improved function indicates that this choice was not optimal. ROS does not need to be a regulator of 8-nitro-cGMP; its sufficient and necessary role in 8-nitro-cGMP production is established via its sufficient and necessary role for NO and cGMP production (via the linear pathway ROS→NIA1/2→NO→NOGC1→cGMP). In addition, assuming ROS to be a direct and necessary regulator of 8-nitro-cGMP contradicts the evidence that NO (which does not lead to ROS production [49]) is sufficient for 8-nitro-cGMP production.

PP2CA* = !RCARs
Original: PP2CA* = !RCARs & !ROS
Interpretation: The 2017 model assumed that ROS inhibits PP2CA because of the evidence that ROS inhibits ABI1, ABI2 and HAB1. The loss of the regulation by ROS, shared by both GA-improved models, suggests that this assumption is not necessary.

QUAC1* = OST1
Original: QUAC1* = Ca^{2+}_c & OST1
Both models omit the regulatory effect of cytosolic Ca^{2+} on the QUAC1 anion channel. This makes the function easier to satisfy and makes sustained QUAC1=1 possible in GA1-A. The 2017 model assumed that Ca^{2+}_c regulates QUAC1 based on the loss of Ca^{2+}-induced closure for QUAC1 KO reported in [82]. Both GA1-A and GA1-B recapitulate this observation without having the edge. The lack of necessity for the direct regulation is supported by the experimental observation in [83] of anion current through QUAC1 in response to ABA when the Ca^{2+} level was clamped to 110 nM (which corresponds to the resting Ca^{2+}_c level).

The function of SLAC1 is easier to satisfy.
The published model’s regulatory function for SLAC1 incorporated 9 documented direct regulators of the SLAC1 ion channel as well as indirect evidence that MPK9/12 knockout impairs Ca^{2+}_c-induced activation of SLAC1. The three CPK nodes were assumed to be interchangeable (were connected by “or”); all the other regulators were assumed to be necessary, meaning that the regulatory function of SLAC1 contained three 8-variable disjunctive (‘and’-connected) clauses. The improved models have 4-5 clauses and have fewer (5-7) variables included in each clause.

AnionEM* = QUAC1 & SLAC1

Original: AnionEM* = QUAC1 & SLAH3 | SLAC1
This function omits SLAH3 and makes SLAC1 and QUAC1 necessary for AnionEM. This shared modification of the improved models suggests that although SLAH3 is a valid anion channel, its contribution to AnionEM is much weaker than that of the other two. This prediction is consistent with the finding that SLAH3 knockout does not diminish ABA-induced stomatal closure [84]. The Boolean function of the published model, which assumed that QUAC1 and SLAH3 together can lead to sufficient anion efflux, was suboptimal, as it contradicted the experimental finding that SLAC1 KO eliminated ABA-induced closure [85].

S1 Table. The scoring functions used in our workflow

The scoring function indicates the average value of the respective node in the trap spaces of the model on the x axis and the score on the y axis.

Category	Scoring function	Examples
ON	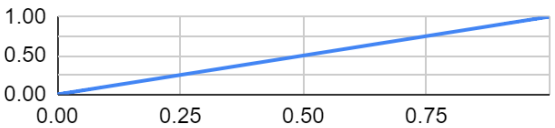	ABA=1, observing pH_c.
Some/ON	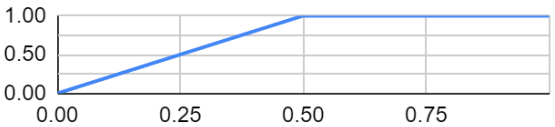	NO CA, observing Closure. The closure (i.e., reduction in the stomatal aperture) in various reported experiments varied between 30% and 60% of that in response to ABA.
Some	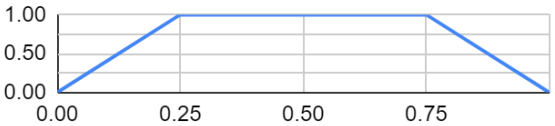	8-nitro-cGMP CA, observing Closure. The experimental closure response was around 25% of the response to ABA.
OFF/Some	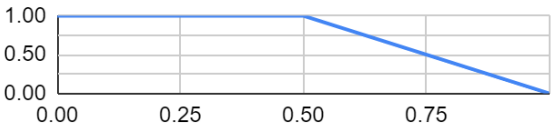	ABA=1, S1P/PhytoS1P KO, observing Closure. S1P was depleted using a chemical, whose effect may reduce over time. Thus, the experimentally observed weak closure (instead of the expected lack of closure) may be due to the dissipation of the depletion.
OFF	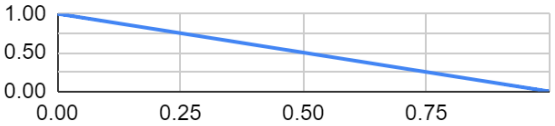	NO CA, observing ROS.

S2 Table. Detailed benchmark results

The starting accuracies and the final accuracies are averages of 5 independent runs. We used models from the Cell Collective with size (N) less than 30. We generated artificial training sets of size 10N, from which a randomly selected 8N were used as the training set,

and the remaining 2N were used as the validation set. The accuracy is calculated by dividing the score of the model by the respective maximal score. The standard deviation is shown in parentheses.

model name	size (N)	training start (%)	training final (%)	validation start (%)	validation final (%)
Arabidopsis thaliana Cell Cycle	14	13.7(±11.3)	93.1(±2.2)	7.5(±8)	87.4(±3.5)
Aurora Kinase A in Neuroblastoma	23	38.8(±17)	98.2(±1.9)	37(±20.1)	95.6(±5.6)
B cell differentiation	22	44.2(±11.8)	99.3(±1.3)	44.7(±15)	98.4(±1.5)
BT474 Breast Cell Line Long-term ErbB Network	24	49.9(±13.8)	99.5(±0.8)	50.5(±6.4)	95.2(±4.6)
BT474 Breast Cell Line Short-term ErbB Network	16	49.9(±9.9)	100(±0)	46.1(±17.5)	96.4(±4)
Budding Yeast Cell Cycle	20	60.7(±11.4)	99.4(±0.8)	55.1(±18.4)	95(±4.5)
Budding Yeast Cell Cycle 2009	18	23.7(±19.4)	92.8(±4.6)	18.8(±17.1)	84.3(±5.2)
CD4+ T Cell Differentiation and Plasticity	18	41.9(±5.8)	96.3(±1.7)	44.1(±13.1)	84.5(±6.2)
Cardiac development	15	67.3(±5.7)	100(±0)	72(±12.6)	97.7(±3.2)
Cell Cycle Transcription by Coupled CDK and Network Oscillators	9	39.9(±21.9)	100(±0)	30.8(±26.6)	100(±0)
Cortical Area Development	5	74.8(±11.2)	99.5(±1.1)	73.3(±13.2)	93(±4.5)
Death Receptor Signaling	28	50.9(±12.4)	97(±4.1)	43.4(±15.6)	96.6(±4.6)
FA BRCA pathway	28	29.9(±16.9)	94.2(±2.9)	25.1(±14.9)	87.2(±4.1)
FGF pathway of Drosophila Signalling Pathways	23	79.9(±9)	100(±0)	78.7(±9.6)	98.7(±2.9)
Fanconi anemia and checkpoint recovery	15	38.5(±7.5)	96.5(±2.5)	37(±7.1)	79.7(±9.3)
HCC1954 Breast Cell Line Long-term ErbB Network	23	61.8(±6.4)	99.1(±1.4)	64.4(±8.3)	97.4(±2.1)
HCC1954 Breast Cell Line Short-term ErbB Network	16	49.8(±6.6)	99.9(±0.2)	49(±13)	97.2(±1.6)
HH Pathway of Drosophila Signaling Pathways	24	60.1(±11)	98.6(±1.9)	61.2(±13.4)	95(±6.7)
Human Gonadal Sex Determination	19	50.3(±16.1)	97.5(±2.5)	45.8(±21.2)	89.7(±9.3)
Iron acquisition and oxidative stress response in aspergillus fumigatus	22	49.2(±30.2)	99.2(±1.5)	49.1(±30.5)	96.6(±2.1)
Lac Operon	13	39(±17.9)	99.4(±0.9)	29.6(±22.3)	97.3(±4.2)
Mammalian Cell Cycle	20	32.5(±10.6)	98.1(±1.4)	25(±14.8)	90(±5.1)
Mammalian Cell Cycle 2006	10	30.8(±11)	98.9(±1.1)	28.7(±9.5)	94.5(±4.5)
Metabolic Interactions in the Gut Microbiome	12	77.1(±7.6)	99.6(±0.9)	74.8(±13.6)	92.5(±8.4)

Neurotransmitter Signaling Pathway	16	38(±18.1)	100(±0)	36.3(±16.7)	100(±0)
Oxidative Stress Pathway	19	41.7(±11.6)	99.7(±0.4)	42.2(±3.2)	99.7(±0.6)
Predicting Variabilities in Cardiac Gene	15	69.9(±3.8)	99.8(±0.4)	65.3(±11.9)	95.3(±7)
Pro-inflammatory Tumor Microenvironment in Acute Lymphoblastic Leukemia	26	50.2(±10.2)	94(±7.8)	47.9(±12.8)	91.2(±7.3)
Processing of Spz Network from the Drosophila Signaling Pathway	24	51.6(±12.2)	99.5(±0.9)	51.7(±12.4)	97.9(±2.9)
Regulation of the L-arabinose operon of Escherichia coli	13	45.9(±19.8)	100(±0)	43.6(±23.3)	100(±0)
SKBR3 Breast Cell Line Long-term ErbB Network	25	47.7(±7.2)	99.5(±0.6)	46.8(±8)	95.3(±4.8)
SKBR3 Breast Cell Line Short-term ErbB Network	16	50.6(±8.6)	100(±0)	44.8(±8.4)	97.8(±1.8)
Septation Initiation Network	30	54.5(±9.8)	99.3(±0.5)	49.5(±7.9)	98.4(±1.2)
T cell differentiation	23	63.1(±9.9)	100(±0)	55(±11.5)	99.2(±0.8)
T-LGL Survival Network 2011 Reduced Network	18	29.6(±21)	99.2(±1.8)	27.5(±19.1)	98(±2.8)
TOL Regulatory Network	24	60.6(±18.4)	97.7(±1.3)	57.5(±20.9)	91.3(±3.1)
Toll Pathway of Drosophila Signaling Pathway	11	40.2(±6.8)	100(±0)	36.4(±8.5)	100(±0)
Trichostrongylus retortaeformis	26	34.9(±15.4)	98.6(±1.3)	32(±11.9)	93.3(±5.8)
VEGF Pathway of Drosophila Signaling Pathway	18	73.2(±16.2)	100(±0)	69.4(±21.8)	100(±0)
Wg Pathway of Drosophila Signalling Pathways	26	69(±19.7)	100(±0)	72.1(±21.7)	98.8(±1.7)

S3 Table. The full name of the abbreviated node names in the ABA-induced closure models

Most of these node names are adopted from the 2017 ABA-induced closure model [29]. We also indicate the node names used in the code and in Figure 5, when they are different from the original name.

Node name in the network	Node name used in the code	Node name in Figure 5	Full name
8-nitro-cGMP		8ncGMP	8-nitro-cyclic guanosine monophosphate
ABA			Abscisic acid
ABH1		(not shown)	ABA hypersensitive
ABI1			ABA (abscisic acid)-insensitive 1
ABI2			ABA (abscisic acid)-insensitive 2
Actin Reorganization	Actin_Reorganization	AR	Actin reorganization
ADPRc		(not shown)	ADP (adenosine diphosphate)-ribosyl cyclase

AnionEM			Anion efflux through the plasma membrane
Aquaporin(PIP2;1)	AquaporinPIP2_1	Aquapor	Plasma membrane intrinsic protein 2;1 (Aquaporin)
ARP Complex	ARP_Complex	(not shown)	Actin related protein complex
AtRAC1			small GTPase RAC1
Ca^{2+}_c	Ca2c	Ca^{2+}	Cytosolic calcium
Ca^{2+} ATPase	Ca2_ATPase	(not shown)	Ca^{2+} ATPases and Ca^{2+}/H^+ antiporters responsible for Ca^{2+} efflux from the cytosol
cADPR			cyclic ADP-ribose
CaIM			Ca^{2+} influx across the plasma membrane
cGMP		(not shown)	Cyclic guanosine monophosphate
CIS			Ca^{2+} influx to the cytosol from intracellular stores
Closure			Stomatal closure
CPK23		(not shown)	Calcium-dependent protein kinase 23
CPK3/21	CPK3_21		Calcium-dependent protein kinases 3 and 21
CPK6		(not shown)	Calcium-dependent protein kinase 6
DAG		(not shown)	Diacylglycerol
DAGK		(not shown)	Diacylglycerol kinase
Depolarization		Depolar	Plasma membrane depolarization
ERA1		(not shown)	Enhanced Response to Abscisic acid1
GAPC1/2	GAPC1_2	(not shown)	Glyceraldehyde-3-phosphate dehydrogenase subunits 1 and 2
GCR1		(not shown)	putative G protein–coupled receptor
GEF1/4/10	GEF1_4_10	(not shown)	Guanine exchange factors 1, 4 and 10
GHR1			Guard cell hydrogen peroxide resistant 1
GPA1			Heterotrimeric G protein α subunit 1
GTP		(not shown)	Guanosine 5'-triphosphate
H^+ ATPase	H_ATPase		H^+ ATPase at the plasma membrane
H_2O Efflux	H2O_Efflux	H_2O eff	water efflux through the plasma membrane
HAB1			Hypersensitive to ABA 1
InsP3			Inositol-1,4,5 trisphosphate
InsP6		(not shown)	Inositol hexakisphosphate
K^+ Efflux	K_efflux	K^+ eff	K^+ efflux through the plasma membrane
KEV			K^+ efflux from the vacuole to the cytosol
KOUT			K^+ efflux through slowly activating outwardly-rectifying K^+ channels through the plasma membrane
Malate			Malate
Microtubule Depolymerization	Microtubule_Depolymerization	MD	Microtubule depolymerization
MPK9/12	MPK9_12		Mitogen-activated protein kinases 9 and 12
MRP5		(not shown)	Multidrug Resistance-associated Protein 5
NAD^+	NAD	(not shown)	Nicotinamide adenine dinucleotide
NADPH		(not shown)	Nicotinamide adenine dinucleotide phosphate

NIA1/2	NIA1_2	(not shown)	Nitrate reductase 1/2
Nitrite		(not shown)	Nitrite
NO			Nitric Oxide
NOGC1		(not shown)	Nitric Oxide dependent Guanylate Cyclase
NtSyp121		(not shown)	Tobacco syntaxin-like SNARE (soluble N-ethylmaleimide-sensitive factor) attachment protein receptors
OST1			protein kinase OPEN STOMATA 1
PA			Phosphatidic acid
PC		(not shown)	Phosphatidyl Choline
PEPC		(not shown)	Phosphoenolpyruvate carboxylase
pHc			Increase of the cytosolic pH level
PI3P5K		(not shown)	Phosphatidylinositol 3-phosphate 5-kinase
PLC		(not shown)	Phospholipase C
PLDα	PLDalpha		Phospholipase D α1
PLDδ	PLDdelta		Phospholipase D δ
PP2CA			Protein Phosphatase 2CA
PtdIns(3,5)P2	PtdIns3_5P2	(not shown)	Phosphatidylinositol 3,5-bisphosphate
PtdIns(4,5)P2	PtdIns4_5P2	(not shown)	Phosphatidylinositol 4,5-bisphosphate
PtdInsP3		(not shown)	Phosphatidylinositol 3-phosphate
PtdInsP4		(not shown)	Phosphatidylinositol 4-phosphate
QUAC1			QUickly activating Anion Channel1
RBOH			NADPH oxidases AtRBOH D and F
RCARs			Regulatory Components of ABA Receptor
RCN1		(not shown)	Protein phosphatase 2A
ROP11		(not shown)	Small GTPase ROP11
ROS			Reactive oxygen species
SACC		(not shown)	Stretch activated calcium channels
S1P / PhytoS1P	S1P_PhytoS1P	S1P	sphingosine-1-phosphate/ phyto sphingosine-1-phosphate
SCAB1		(not shown)	Stomatal Closure-related Actin Binding protein
SLAC1			Slow Anion Channel- associated 1
SLAH3			SLAC1 Homologue 3
Sph		(not shown)	Sphingosine
SPHK1/2	SPHK1_2	(not shown)	Sphingosine Kinases 1 and 2
SPP1		(not shown)	Sphingoid Phosphate Phosphatase 1
TCTP		(not shown)	Translationally controlled tumor protein
V-ATPase		(not shown)	Vacuolar proton ATPase
Vacuolar Acidification	Vacuolar_Acidification	VA	Vacuolar Acidification
V-PPase		(not shown)	vacuolar proton pyrophosphatase

S4 Table. Compilation of experimental results used to score the ABA-induced closure model

In our compilation of 505 experiments 244 assayed stomatal aperture and 261 assayed other nodes of the network.

The foundational experiment performed to investigate ABA-induced stomatal closure is to provide 20-50 μM ABA to leaf epidermal peels that were pre-incubated in a solution that opened stomata. The aperture of a population of stomata (usually hundreds) before and

after treatment is measured used to establish that ABA induces a significant aperture reduction (i.e., closure). The apertures of a population of stomata under a mock treatment consisting of the solution used to deliver ABA (usually ethanol) are measured as a negative control (to establish that no closure happens).

There are two main types of experimental interventions: the genetic or pharmacological knockout of an element of the network (node) in the presence of ABA, and the external supply or activation of a node in the absence of ABA. Combinatorial interventions usually consist of providing either ABA or a node that was documented to induce stomatal closure combined with the knockout of one or multiple additional nodes. We represent the external supply or activation as “CA” (constitutive activation), and implement it as keeping the node in the ON state. We represent knockout as “KO” and implement it by keeping the node in the OFF state.

One type of experiment required a more subtle representation. Ca^{2+} flow through the plasma membrane (represented by the node CaIM) can be mediated by stretch-activated channels or ROS-activated channels. Certain experiments that measured Ca^{2+} flow through the membrane were not set up to monitor stretch-activated channels. To represent these experiments, we introduced the node SACC to represent stretch-activated channels, made it a regulator of the node CaIM, and assumed that it is inactive in the setting that represents the experiment.

As described in the Methods, the extent of reduction in the stomatal apertures in response to ABA serves as the benchmark to categorize the effect of experimental interventions. Reductions similar in magnitude to the reduction in response to ABA are categorized as “ON”, the lack of reduction observed for mock treatment defines the “OFF” category, and intermediate reductions are categorized as “Some”. Certain experiments (at least 80) were reported in multiple publications, and a fraction of these reported contradictory findings. We accommodate this variability by using the classifications OFF/Some and Some/ON. As indicated in S1 Table, a range of model results are deemed consistent with such a hybrid classification, e.g., from 0.5 to 1 for Some/ON. Altogether, there are 248 cases of OFF, 53 cases of OFF/Some, 42 cases of Some, 53 cases of Some/ON and 111 cases of ON in our compilation.

All references are given in PMID, with the only exception of Qu et al. (doi.org/10.1007/s10725-017-0353-5). The key perturbations that lead to stomatal closure in the absence of ABA are underlined and italicized. Experimental observations in the presence of ABA are shown in gray background.

ID	Source	Perturbation	Experimental result	Observed node	Category	Reference PMIDs
1	ABA=0	WT	no closure	Closure	OFF	
2	ABA=1	WT	closure	Closure	ON	
3	ABA=0	*ROS CA*	closure(>50%)	Closure	ON	12773379, 21719691, 22589465, 12446847, 22730405, 21262908, 16367958, 19690149
4	ABA=0	RBOH KO	no closure	Closure	OFF	12773379, 15064385
5	ABA=0	RBOH KO, *ROS CA*	closure(>50%)	Closure	ON	12773379,

						16367958
6	ABA=0	ROS KO	no closure	Closure	OFF	11500543, 16367958
7	ABA=1	ROS KO	no, reduced closure	Closure	OFF/Some	11500543, 16367958
8	ABA=1	RBOH KO	reduced closure no closure	Closure	OFF/Some	12773379, 16367958, 15064385, 19690149
9	ABA=1	PLDα KO, RBOH KO	no closure	Closure	OFF	19690149
10	ABA=0	*CaIM CA*	closure(>50%)	Closure	ON	16664518, 21719691
11	ABA=0	Ca^{2+}_{c} KO	no closure	Closure	OFF	19302418, 24271006, 15064385, 18721267
12	ABA=1	Ca^{2+}_{c} KO	reduced closure /no closure	Closure	OFF/Some	19302418, 24271006, 15064385 /18721267
13	ABA=0	SCAB1 CA	no closure	Closure	OFF	21719691
14	ABA=1	SCAB1 CA	slower closure	Closure	Some/ON	21719691
15	ABA=1	SCAB1 CA	slower actin reorganization	Actin Reorganization	Some/ON	21719691
16	ABA=0	SCAB1 KO	no closure	Closure	OFF	21719691
17	ABA=1	SCAB1 KO	slower closure	Closure	Some/ON	21719691
18	ABA=1	SCAB1 KO	slower actin reorganization	Actin Reorganization	Some/ON	21719691
19	ABA=0	*ROS CA*, SCAB1 KO	some closure	Closure	Some	21719691
20	ABA=0	*CaIM CA*, SCAB1 KO	some closure	Closure	Some	21719691
21	ABA=0	GEF1/4/10 KO	no closure	Closure	OFF	22908257
22	ABA=1	GEF1/4/10 KO	increased closure	Closure	ON	22908257, 22500990
23	ABA=1	GEF1/4/10 CA	reduced closure, closure	Closure	Some/ON	22500990
24	ABA=0	SPHK1/2 KO	no closure	Closure	OFF	18557834
25	ABA=1	SPHK1/2 KO	reduced closure	Closure	Some	18557834
26	ABA=0	SPHK1/2 CA	no closure	Closure	OFF	18557834
27	ABA=1	SPHK1/2 CA	increased closure	Closure	ON	18557834
28	ABA=0	ABI1 KO	no closure	Closure	OFF	16798945, 16614222, 19690149
29	ABA=1	ABI1 KO	increased closure /closure	Closure	ON	16798945 /16614222, 19690149
30	ABA=0	HAB1 KO	no closure	Closure	OFF	16798945
31	ABA=1	HAB1 KO	increased closure	Closure	ON	16798945
32	ABA=0	ABI1 KO, HAB1 KO	no closure	Closure	OFF	16798945
33	ABA=1	ABI1 KO, HAB1 KO	increased closure	Closure	ON	16798945
34	ABA=0	ABI1 KO, *ROS CA*	closure	Closure	ON	19690149
35	ABA=0	ABI1 KO, *NO CA*	closure	Closure	ON	19690149
36	ABA=0	ABI1 CA	no closure	Closure	OFF	10488243, 16614222, 12446847,

						19690149
37	ABA=1	ABI1 CA	no closure	Closure	OFF	10488243, 16614222, 12446847, 19690149
38	ABA=0	ABI1 CA, *ROS CA*	no closure	Closure	OFF	19690149
39	ABA=0	ABI2 KO	no closure	Closure	OFF	11208021
40	ABA=1	ABI2 KO	closure	Closure	ON	11208021
41	ABA=0	ABI2 CA	no closure	Closure	OFF	11208021, 10488243, 12446847
42	ABA=1	ABI2 CA	no closure	Closure	OFF/Some	11208021, 10488243, 12446847
43	ABA=0	RCARs CA	no closure	Closure	OFF	25969135
44	ABA=1	RCARs CA	increased closure	Closure	ON	25969135
45	ABA=0	RCARs KO	no closure	Closure	OFF	19874541
46	ABA=1	RCARs KO	reduced closure	Closure	Some	19874541
47	ABA=0	*CaIM CA*, RCARs KO	some closure, closure	Closure	Some/ON	19874541
48	ABA=0	GCR1 KO	no closure	Closure	OFF	15155892
49	ABA=1	GCR1 KO	increased closure	Closure	ON	15155892
50	ABA=0	TCTP CA	no closure	Closure	OFF	22610367
51	ABA=1	TCTP CA	increased closure	Closure	ON	22610367
52	ABA=0	S1P/PhytoS1P KO	no closure	Closure	OFF	11279499
53	ABA=1	S1P/PhytoS1P KO	no, reduced closure	Closure	OFF/Some	11279499
54	ABA=0	OST1 KO	no closure	Closure	OFF	24033256, 31179540, 15064385
55	ABA=1	OST1 KO	no closure	Closure	OFF	24033256, 30361234, 31179540, 15064385
56	ABA=0	OST1 CA	no closure	Closure	OFF	24033256
57	ABA=1	OST1 CA	increased closure	Closure	ON	24033256
58	ABA=0	ERA1 KO	no, some closure	Closure	OFF/Some	9765153
59	ABA=1	ERA1 KO	increased closure	Closure	ON	9765153
60	ABA=0	ABH1 KO	no, some closure	Closure	OFF/Some	11525733
61	ABA=1	ABH1 KO	increased closure	Closure	ON	11525733
62	ABA=0	PLDα KO	no closure	Closure	OFF	16614222, 22932846, 19690149, Qu et al., 24271006, 19690149
63	ABA=1	PLDα KO	no closure reduced closure reduced closure	Closure	OFF/Some	16614222, 19690149, Qu et al., 19690149, 24271006, 22392280
64	ABA=0	PLDα KO, *ROS CA*	closure	Closure	ON	19690149, 22392280

65	ABA=0	PLDδ KO	no closure	Closure	OFF	22589465, 22932846, 22392280
66	ABA=1	PLDδ KO	no closure reduced closure, closure	Closure	OFF	22589465, 22392280
67	ABA=0	PLDδ KO, *ROS CA*	no closure closure	Closure	OFF	22589465, 22392280
68	ABA=0	*PA CA*	some closure, closure	Closure	Some/ON	10518598, 16614222, 24271006, Qu et al., 22392080
69	ABA=1	*PA CA*	closure	Closure	ON	10518598
70	ABA=0	PLDα KO, PLDδ KO	no closure	Closure	OFF	10518598, 22932846, 22392280
71	ABA=1	PLDα KO, PLDδ KO	reduced closure	Closure	Some	10518598, 22392280
72	ABA=0	PLDα KO, PLDδ KO, *ROS CA*	some closure, closure	Closure	Some/ON	22392280
73	ABA=0	*PA CA*, PLDα KO, PLDδ KO	closure (more than PA CA) some closure (same as PA CA)	Closure	Some/ON	10518598, 22392080
74	ABA=0	DAG CA	no closure	Closure	OFF	10518598
75	ABA=0	ABI1 KO, *PA CA*	some closure, closure	Closure	Some/ON	16614222
76	ABA=0	ABI1 CA, *PA CA*	no closure	Closure	OFF	16614222
77	ABA=0	*PA CA*, PLDα KO	some closure, closure	Closure	Some/ON	16614222, 24271006, 22392080
78	ABA=0	*PA CA*, PLDδ KO	some closure, closure	Closure	Some/ON	22392080
79	ABA=0	GPA1 KO, *PA CA*	some closure, closure	Closure	Some/ON	16614222
80	ABA=0	GPA1 KO, *PA CA*, PLDα KO	some closure, closure	Closure	Some/ON	16614222
81	ABA=0	ABI1 KO, PLDα KO	no closure	Closure	OFF	16614222
82	ABA=1	ABI1 KO, PLDα KO	closure	Closure	ON	16614222
83	ABA=0	GPA1 KO	no closure	Closure	OFF	16614222, 12789341
84	ABA=1	GPA1 KO	closure	Closure	ON	16614222, 11408655, 12789341
85	ABA=0	GPA1 KO, PLDα KO	no closure	Closure	OFF	16614222
86	ABA=1	GPA1 KO, PLDα KO	no closure	Closure	OFF	16614222
87	ABA=0	PP2CA KO	no closure	Closure	OFF	Qu et al., 16361522
88	ABA=0	*PA CA*, PP2CA KO	some closure, closure (less than PA CA)	Closure	Some/ON	Qu et al.
89	ABA=0	Ca^{2+}_c KO, PLDα KO	no closure	Closure	OFF	24271006
90	ABA=1	Ca^{2+}_c KO, PLDα KO	no, reduced closure	Closure	OFF/Some	24271006
91	ABA=0	*PA CA*, Ca^{2+}_c KO	some closure, closure	Closure	Some/ON	24271006
92	ABA=0	*PA CA*, Ca^{2+}_c KO, PLDα KO	some closure, closure	Closure	Some/ON	24271006
93	ABA=0	CPK3/21 KO	no closure	Closure	OFF	17032064, 21994053
94	ABA=1	CPK3/21 KO	reduced closure, closure	Closure	Some/ON	17032064
95	ABA=0	CPK6 KO	no closure	Closure	OFF	17032064,

						21994053
96	ABA=1	CPK6 KO	reduced closure, closure	Closure	Some/ON	17032064
97	ABA=0	CPK3/21 KO, CPK6 KO	no closure	Closure	OFF	17032064
98	ABA=1	CPK3/21 KO, CPK6 KO	no, reduced closure	Closure	OFF/Some	17032064
99	ABA=0	cGMP CA	no closure	Closure	OFF	23396828
100	ABA=1	NOGC1 KO, cGMP CA	reduced closure, closure	Closure	Some/ON	23396828
101	ABA=0	cADPR KO	no closure no, some closure /some closure	Closure	OFF/Some	9861057, 10518598 /19847112
102	ABA=1	cADPR KO	slower closure /reduced closure	Closure	Some/ON	9861057 /19847112, 10518598
103	ABA=0	ADPRc KO	no closure	Closure	OFF	9861057
104	ABA=1	ADPRc KO	no, reduced closure	Closure	OFF/Some	9861057
105	ABA=0	PI3P5K KO	no closure	Closure	OFF	23757398
106	ABA=1	PI3P5K KO	reduced, slower closure	Closure	Some/ON	23757398
107	ABA=0	V-ATPase KO	no closure	Closure	OFF	23757398
108	ABA=1	V-ATPase KO	reduced, slower closure	Closure	Some/ON	23757398
109	ABA=0	V-PPase KO	no closure	Closure	OFF	23757398
110	ABA=1	V-PPase KO	reduced, slower closure	Closure	Some/ON	23757398
111	ABA=0	Vacuolar Acidification KO	no closure	Closure	OFF	23757398
112	ABA=1	Vacuolar Acidification KO	reduced closure	Closure	Some	23757398
113	ABA=0	PLC KO	no closure /some closure	Closure	OFF/Some	9990101, 17996010, 10518598 /19847112
114	ABA=1	PLC KO	reduced closure /closure	Closure	Some/ON	9990101, 10518598 /19847112
115	ABA=0	InsP3 KO	no closure	Closure	OFF	9990101
116	ABA=1	InsP3 KO	no, reduced closure	Closure	OFF/Some	9990101
117	ABA=1	PLDα KO, PLDδ KO, cADPR KO	no closure	Closure	OFF	10518598
118	ABA=1	PLC KO, PLDα KO, PLDδ KO	no, reduced closure	Closure	OFF/Some	10518598
119	ABA=1	PLC KO, cADPR KO	no closure	Closure	OFF	10518598
120	ABA=1	PLC KO, PLDα KO, PLDδ KO, cADPR KO	no closure	Closure	OFF	10518598
121	ABA=0	pH_c KO	no closure	Closure	OFF	16968132, 18721267, 15064385
122	ABA=1	pH_c KO	reduced closure no, reduced closure /no closure	Closure	OFF/Some	11408655, 18721267, 15064385 /16968132
123	ABA=0	OST1 KO, pH_c KO	no closure	Closure	OFF	15064385
124	ABA=1	OST1 KO, pH_c KO	no closure	Closure	OFF	15064385
125	ABA=1	GPA1 KO, pH_c KO	no, reduced closure	Closure	OFF/Some	11408655
126	ABA=0	*NO CA*, RBOH KO	closure	Closure	ON	16367958
127	ABA=0	PtdInsP4 KO	no closure	Closure	OFF	12368494
128	ABA=1	PtdInsP4 KO	no, reduced closure	Closure	OFF/Some	12368494

129	ABA=0	PtdInsP3 KO	no closure	Closure	OFF	12368494
130	ABA=1	PtdInsP3 KO	no, reduced closure	Closure	OFF/Some	12368494
131	ABA=1	PtdInsP3 KO, PtdInsP4 KO	no, reduced closure	Closure	OFF/Some	12368494 17160388
132	ABA=0	ROP11 CA	no closure	Closure	OFF	22233300
133	ABA=1	ROP11 CA	reduced closure	Closure	Some	22233300
134	ABA=0	ROP11 KO	no closure	Closure	OFF	22233300
135	ABA=1	ROP11 KO	increased closure	Closure	ON	22233300
136	ABA=0	KOUT KO	no closure	Closure	OFF	12671068, 15064385
137	ABA=1	KOUT KO	reduced closure	Closure	Some	12671068, 15064385
138	ABA=0	K^+ efflux KO	no closure	Closure	OFF	12671068
139	ABA=1	K^+ efflux KO	reduced closure	Closure	Some	12671068
140	ABA=0	KOUT KO	no ROS	ROS	OFF	15064385
141	ABA=1	KOUT KO	ROS	ROS	ON	15064385
142	ABA=0	KOUT KO, pH_c KO	no closure	Closure	OFF	15064385
143	ABA=1	KOUT KO, pH_c KO	reduced closure	Closure	Some	15064385
144	ABA=0	PP2CA CA	no closure	Closure	OFF	16361522
145	ABA=1	PP2CA CA	reduced closure	Closure	Some	16361522
146	ABA=1	PP2CA KO	increased closure	Closure	ON	16361522, Qu et al.
147	ABA=0	H^+ ATPase CA	no closure	Closure	OFF	24367097
148	ABA=1	H^+ ATPase CA	reduced closure	Closure	Some	24367097
149	ABA=0	*AtRAC1 KO*	some closure, closure	Closure	Some/ON	11459830
150	ABA=0	AtRAC1 CA	no closure	Closure	OFF	11459830
151	ABA=1	AtRAC1 CA	reduced closure	Closure	Some	11459830
152	ABA=0	QUAC1 KO	no closure	Closure	OFF	20626656
153	ABA=1	QUAC1 KO	no, reduced closure	Closure	OFF/Some	20626656
154	ABA=0	*CaIM CA*, QUAC1 KO	no closure	Closure	OFF	20154005
155	ABA=0	GAPC1/2 KO	no closure	Closure	OFF	22589465
156	ABA=1	GAPC1/2 KO	reduced closure	Closure	Some	22589465
157	ABA=0	GAPC1/2 KO, *ROS CA*	some closure	Closure	Some	22589465
158	ABA=0	GAPC1/2 KO, PLDδ KO	no closure	Closure	OFF	22589465
159	ABA=1	GAPC1/2 KO, PLDδ KO	no, reduced closure	Closure	OFF/Some	22589465
160	ABA=0	GAPC1/2 KO, PLDδ KO, *ROS CA*	no, some closure	Closure	OFF/Some	22589465
161	ABA=0	MPK9/12 KO	no closure	Closure	OFF	19910530
162	ABA=1	MPK9/12 KO	no closure	Closure	OFF/Some	19910530
163	ABA=0	MPK9/12 KO, *ROS CA*	some closure	Closure	Some	19910530
164	ABA=0	SLAC1 KO	no closure	Closure	OFF	18305484
165	ABA=1	SLAC1 KO	no closure	Closure	OFF	18305484
166	ABA=0	ARP Complex KO	no, some closure	Closure	OFF/Some	22570440
167	ABA=1	ARP Complex KO	no, reduced closure	Closure	OFF/Some	22570440
168	ABA=0	ARP Complex KO, *CaIM CA*	some closure	Closure	Some	22570440
169	ABA=0	ARP Complex KO	no actin reorganization	Actin Reorganization	OFF	22570440
170	ABA=1	ARP Complex KO	no, reduced actin	Actin Reorganization	OFF/Some	22570440

			reorganization			
171	ABA=0	Aquaporin(PIP2;1) KO	no closure	Closure	OFF	26163575
172	ABA=1	Aquaporin(PIP2;1) KO	reduced closure	Closure	Some	26163575
173	ABA=0	GHR1 KO	no closure	Closure	OFF	22730405, 30361234
174	ABA=1	GHR1 KO	no closure	Closure	OFF	22730405, 30361234
175	ABA=0	GHR1 KO, *ROS CA*	no closure	Closure	OFF	30361234, 22730405
176	ABA=0	OST1 KO, *ROS CA*	some closure /closure (same as ROS CA)	Closure	Some/ON	30361234 /22730405
177	ABA=0	*CaIM CA*, GHR1 KO	closure	Closure	ON	22730405
178	ABA=0	RCN1 KO	no, some closure	Closure	OFF/Some	12417706
179	ABA=1	RCN1 KO	reduced closure	Closure	Some	12417706
180	ABA=0	SPP1 KO	no closure	Closure	OFF	21910031
181	ABA=1	SPP1 KO	increased closure	Closure	ON	21910031
182	ABA=0	NIA1/2 KO	no, some closure	Closure	OFF/Some	12446847
183	ABA=1	NIA1/2 KO	no closure	Closure	OFF	12446847, 16367958
184	ABA=0	Microtubule Depolymerization KO	no closure	Closure	OFF	24271006, Qu et al.
185	ABA=1	Microtubule Depolymerization KO	no, reduced closure	Closure	OFF/Some	24271006, Qu et al.
186	ABA=0	Microtubule Depolymerization CA	no closure	Closure	OFF	24271006, Qu et al.
187	ABA=1	Microtubule Depolymerization CA	closure	Closure	ON	24271006, Qu et al.
188	ABA=0	Microtubule Depolymerization CA, PLDα KO	no closure	Closure	OFF	24271006, Qu et al.
189	ABA=1	Microtubule Depolymerization CA, PLDα KO	reduced closure, closure	Closure	Some/ON	24271006, Qu et al.
190	ABA=0	Microtubule Depolymerization CA, PP2CA KO	no closure	Closure	OFF	Qu et al.
191	ABA=1	Microtubule Depolymerization CA, PP2CA KO	increased closure	Closure	ON	Qu et al.
192	ABA=0	Microtubule Depolymerization KO, PLDα KO	no closure	Closure	OFF	Qu et al.
193	ABA=1	Microtubule Depolymerization KO, PLDα KO	no closure	Closure	OFF	Qu et al.
194	ABA=0	Microtubule Depolymerization KO, PP2CA KO	no closure	Closure	OFF	Qu et al.
195	ABA=1	Microtubule Depolymerization KO, PP2CA KO	closure	Closure	ON	Qu et al.
196	ABA=0	NOGC1 KO	no closure	Closure	OFF	23396828
197	ABA=1	NOGC1 KO	no closure	Closure	OFF	23396828
198	ABA=0	*NO CA*, NOGC1 KO	no closure	Closure	OFF	23396828
199	ABA=0	MRP5 KO	no closure	Closure	OFF	17098742
200	ABA=1	MRP5 KO	reduced closure	Closure	Some	17098742
201	ABA=0	*pH_c CA*	some closure, closure(>50%)	Closure	Some/ON	18721267
202	ABA=1	*pH_c CA*	increased closure	Closure	ON	18721267

203	ABA=0	NO KO	no closure	Closure	OFF	18721267
204	ABA=1	NO KO	no closure	Closure	OFF	18721267, 16367958
205	ABA=1	SLAH3 KO	closure	Closure	ON	21586729
206	ABA=0	NtSyp121 KO	no closure	Closure	OFF	19825544
207	ABA=1	NtSyp121 KO	no closure	Closure	OFF	19825544
208	ABA=0	*S1P/PhytoS1P CA*	some closure, closure(>50%)	Closure	Some/ON	12789341
209	ABA=0	GPA1 KO, *S1P/PhytoS1P CA*	no, some closure	Closure	OFF/Some	12789341
210	ABA=0	Nitrite CA	some closure, closure(>50%)	Closure	Some/ON	12446847
211	ABA=0	Nitrite CA, NIA1/2 KO	no closure	Closure	OFF	12446847
212	ABA=0	*NO CA*	some closure, closure(>50%) /some closure(<25%)	Closure	Some/ON	12446847, 19825544, 17996010, 18721267, 16367958, 19690149 /23396828, 22932846
213	ABA=0	NIA1/2 KO, *NO CA*	some closure, closure(>50%)	Closure	Some/ON	12446847, 16367958
214	ABA=0	NIA1/2 KO, *ROS CA*	closure(>50%) /no, some closure*	Closure	Some/ON	12446847 /16367958
215	ABA=0	*NO CA*, NOGC1 KO, cGMP CA	some closure, closure (similar to NO CA)	Closure	Some/ON	23396828
216	ABA=0	GPA1 KO, *ROS CA*	closure (same as ROS CA)	Closure	ON	21262908
217	ABA=0	Actin Reorganization KO, *ROS CA*	some closure	Closure	Some	24372484
218	ABA=0	*8-nitro-cGMP CA*	some closure(~25%)	Closure	Some	23396828
219	ABA=0	*8-nitro-cGMP CA*, SLAC1 KO	no closure	Closure	OFF	23396828
220	ABA=0	*cADPR CA*	closure(>50%)	Closure	ON	9861057
221	ABA=0	ABI1 CA, *AtRAC1 KO*	some closure, closure	Closure	Some/ON	11459830
222	ABA=0	ABI1 CA, AtRAC1 CA	no closure	Closure	OFF	11459830
223	ABA=0	*InsP3 CA*	some closure, closure(~25%)	Closure	Some/ON	2388697
224	ABA=0	*InsP3 CA*	Ca^{2+}_c oscillation	Ca^{2+}_c	Some	2388697
225	ABA=0	CaIM KO	no closure	Closure	OFF	2388697
226	ABA=0	CaIM KO	no Ca^{2+}_c	Ca^{2+}_c	OFF	2388697
227	ABA=0	CaIM KO, *InsP3 CA*	some closure, closure(~25%)	Closure	Some/ON	2388697
228	ABA=0	CaIM KO, *InsP3 CA*	Ca^{2+}_c oscillation	Ca^{2+}_c	Some	2388697
229	ABA=0	*NO CA*, NtSyp121 KO	some closure	Closure	Some	19825544
230	ABA=0	*NO CA*, PLC KO	no closure	Closure	OFF	17996010
231	ABA=0	*NO CA*, PLDδ KO	no closure	Closure	OFF	22932846
232	ABA=0	*NO CA*, PLDα KO	some closure, closure (same as NO CA)	Closure	Some/ON	22932846, 19690149
233	ABA=0	*NO CA*, PLDα KO, PLDδ KO	no closure	Closure	OFF	22932846
234	ABA=0	*8-nitro-cGMP CA*, cADPR KO	no closure	Closure	OFF	23396828
235	ABA=0	*8-nitro-cGMP CA*, Ca^{2+}_c KO	no, some closure	Closure	OFF/Some	23396828
236	ABA=0	GCR1 KO, *S1P/PhytoS1P CA*	closure(>50%)	Closure	ON	15155892
237	ABA=0	*CaIM CA*, CPK3/21 KO	some closure	Closure	Some	21994053
238	ABA=0	*CaIM CA*, CPK6 KO	some closure	Closure	Some	21994053

239	ABA=0	ABI1 CA, *NO CA*	no closure	Closure	OFF	12446847, 19690149
240	ABA=0	ABI2 CA, *NO CA*	no closure	Closure	OFF	12446847
241	ABA=0	*CaIM CA*, TCTP CA	increased closure compared to CaIM CA	Closure	ON	22610367
242	ABA=0	*CaIM CA*, PLDα KO	no closure	Closure	OFF	24271006
243	ABA=0	NO KO, *ROS CA*	no, some closure	Closure	OFF/Some	16367958
244	ABA=0	*NO CA*, ROS KO	closure	Closure	ON	16367958
245	ABA=0	WT	no ROS	ROS	OFF	23946352, 16367958, 23396828, 15064385, 24033256, 12746515, 19690149, 22730405
246	ABA=1	WT	ROS	ROS	ON	23946352, 16367958, 23396828, 15064385, 24033256, 12746515, 19690149, 22730405, 22392280
247	ABA=0	WT	no NO	NO	OFF	23946352, 18721267, 16367958, 23396828, 19690149
248	ABA=1	WT	NO	NO	ON	23946352, 18721267, 16367958, 23396828, 19690149, 22392280
249	ABA=0	WT	no pH_c	pH_c	OFF	23946352, 18721267, 20739306, 15064385, 22392280
250	ABA=1	WT	pH_c	pH_c	ON	23946352, 18721267, 20739306, 15064385, 22392280
251	ABA=0	RCARs KO	no ROS	ROS	OFF	23946352
252	ABA=1	RCARs KO	no ROS	ROS	OFF	23946352
253	ABA=0	RCARs KO	no NO	NO	OFF	23946352
254	ABA=1	RCARs KO	no NO	NO	OFF	23946352
255	ABA=0	RCARs KO	no pH_c	pH_c	OFF	23946352
256	ABA=1	RCARs KO	no pH_c	pH_c	OFF	23946352
257	ABA=0	NO CA	some pH_c	pH_c	Some	18721267
258	ABA=1	NO CA	pH_c	pH_c	ON	18721267
259	ABA=0	NO KO	no pH_c	pH_c	OFF	18721267
260	ABA=1	NO KO	reduced pH_c	pH_c	Some	18721267

261	ABA=0	Ca^{2+}_c KO	no pH_c	pH_c	OFF	18721267, 15064385
262	ABA=1	Ca^{2+}_c KO	no pH_c /pH_c	pH_c	OFF	18721267 /15064385
263	ABA=0	Ca^{2+}_c KO	no ROS	ROS	OFF	15064385
264	ABA=1	Ca^{2+}_c KO	ROS	ROS	ON	15064385
265	ABA=0	pH_c KO	no NO	NO	OFF	18721267
266	ABA=1	pH_c KO	no NO	NO	OFF	18721267
267	ABA=0	pH_c CA	NO	NO	ON	18721267
268	ABA=1	pH_c CA	NO	NO	ON	18721267
269	ABA=0	Ca^{2+}_c KO	no NO	NO	OFF	18721267
270	ABA=1	Ca^{2+}_c KO	no NO	NO	OFF	18721267
271	ABA=0	ROS CA	NO	NO	ON	16367958, 19690149
272	ABA=0	NIA1/2 KO	no, some NO	NO	OFF/Some	16367958
273	ABA=1	NIA1/2 KO	no NO	NO	OFF	16367958
274	ABA=0	NIA1/2 KO, ROS CA	no NO	NO	OFF	16367958
275	ABA=0	Nitrite CA	NO	NO	ON	16367958
276	ABA=0	NIA1/2 KO, Nitrite CA	no NO	NO	OFF	16367958
277	ABA=0	RBOH KO	no NO	NO	OFF	16367958
278	ABA=1	RBOH KO	no NO	NO	OFF	16367958
279	ABA=0	RBOH KO, ROS CA	NO	NO	ON	16367958
280	ABA=0	ABI1 KO	no NO	NO	OFF	19690149
281	ABA=1	ABI1 KO	NO	NO	ON	19690149
282	ABA=0	NO CA	no ROS	ROS	OFF	16367958
283	ABA=1	NO KO	ROS	ROS	ON	16367958
284	ABA=0	WT	no CaIM	CaIM	OFF	24033256
285	ABA=1	WT	CaIM	CaIM	ON	24033256
286	ABA=0	WT	no SACC	SACC	OFF	24033256
287	ABA=0	SACC KO	no CaIM	CaIM	OFF	21262908
288	ABA=1	SACC KO	CaIM	CaIM	ON	21262908
289	ABA=0	SACC KO, GPA1 KO	no CaIM	CaIM	OFF	21262908
290	ABA=1	SACC KO, GPA1 KO	no CaIM	CaIM	OFF	21262908
291	ABA=0	GPA1 KO	no ROS	ROS	OFF	21262908
292	ABA=1	GPA1 KO	no ROS	ROS	OFF	21262908
293	ABA=0	Aquaporin(PIP2;1) KO	no ROS	ROS	OFF	26163575
294	ABA=1	Aquaporin(PIP2;1) KO	no ROS	ROS	OFF	26163575, 28784763
295	ABA=0	WT	no Aquaporin(PIP2;1)	Aquaporin(PIP2;1)	OFF	28784763
296	ABA=1	WT	Aquaporin(PIP2;1)	Aquaporin(PIP2;1)	ON	28784763
297	ABA=0	OST1 KO	no Aquaporin(PIP2;1)	Aquaporin(PIP2;1)	OFF	28784763
298	ABA=1	OST1 KO	no Aquaporin(PIP2;1)	Aquaporin(PIP2;1)	OFF	28784763
299	ABA=0	WT	no SLAC1	SLAC1	OFF	22730405, 19910530
300	ABA=1	WT	SLAC1	SLAC1	ON	22730405, 19910530

301	ABA=0	OST1 KO	no SLAC1	SLAC1	OFF	22730405
302	ABA=1	OST1 KO	no SLAC1	SLAC1	OFF	22730405
303	ABA=0	GHR1 KO	no SLAC1	SLAC1	OFF	22730405
304	ABA=1	GHR1 KO	no, reduced SLAC1	SLAC1	OFF/Some	22730405
305	ABA=1	ABI1 CA	no pH_c	pH_c	OFF	20739306
306	ABA=1	ABI2 CA	no pH_c	pH_c	OFF	20739306
307	ABA=1	OST1 KO	no pH_c	pH_c	OFF	20739306
308	ABA=0	CaIM CA	pH_c	pH_c	ON	20739306
309	ABA=0	CaIM CA, ABI1 CA	pH_c	pH_c	ON	20739306
310	ABA=0	CaIM CA, ABI2 CA	pH_c	pH_c	ON	20739306
311	ABA=0	CaIM CA, OST1 KO	pH_c	pH_c	ON	20739306
312	ABA=0	PLDα KO, PLDδ KO	no pH_c	pH_c	OFF	22392280
313	ABA=1	PLDα KO, PLDδ KO	no pH_c	pH_c	OFF	22392280
314	ABA=0	WT	no $Ca^{2+}{}_c$	$Ca^{2+}{}_c$	OFF	20739306, 31179540, 22392280
315	ABA=1	WT	$Ca^{2+}{}_c$ oscillation	$Ca^{2+}{}_c$	Some	20739306, 31179540, 22392280
316	ABA=1	pH_c KO	no, reduced $Ca^{2+}{}_c$	$Ca^{2+}{}_c$	OFF/Some	20739306
317	ABA=0	OST1 KO	no $Ca^{2+}{}_c$	$Ca^{2+}{}_c$	OFF	31179540
318	ABA=1	OST1 KO	no $Ca^{2+}{}_c$	$Ca^{2+}{}_c$	OFF	31179540
319	ABA=0	PLDα KO, PLDδ KO	no $Ca^{2+}{}_c$	$Ca^{2+}{}_c$	OFF	22392280
320	ABA=1	PLDα KO, PLDδ KO	$Ca^{2+}{}_c$ oscillation	$Ca^{2+}{}_c$	Some	22392280
321	ABA=0	WT	no actin reorganization	Actin Reorganization	OFF	11459830, 18088331
322	ABA=1	WT	actin reorganization	Actin Reorganization	ON	11459830, 18088331
323	ABA=0	ABI1 CA	no actin reorganization	Actin Reorganization	OFF	11459830
324	ABA=1	ABI1 CA	no actin reorganization	Actin Reorganization	OFF	11459830
325	ABA=0	PtdInsP3 KO	no actin reorganization	Actin Reorganization	OFF	18088331
326	ABA=1	PtdInsP3 KO	no, reduced actin reorganization	Actin Reorganization	OFF/Some	18088331
327	ABA=0	PtdInsP4 KO	no actin reorganization	Actin Reorganization	OFF	18088331
328	ABA=1	PtdInsP4 KO	no, reduced actin reorganization	Actin Reorganization	OFF/Some	18088331
329	ABA=1	PtdInsP3 KO, PtdInsP4 KO	no, reduced actin reorganization	Actin Reorganization	OFF/Some	18088331
330	ABA=1	PLC KO	actin reorganization	Actin Reorganization	ON	18088331
331	ABA=1	ROS KO	no, reduced actin reorganization	Actin Reorganization	OFF/Some	18088331
332	ABA=0	RBOH KO	no actin reorganization	Actin Reorganization	OFF	24372484
333	ABA=1	RBOH KO	no actin reorganization	Actin Reorganization	OFF/Some	24372484
334	ABA=0	WT	AtRAC1	AtRAC1	ON	11459830
335	ABA=1	WT	no AtRAC1	AtRAC1	OFF	11459830
336	ABA=0	ABI1 CA	AtRAC1	AtRAC1	ON	11459830
337	ABA=1	ABI1 CA	AtRAC1	AtRAC1	ON	11459830
338	ABA=0	WT	no 8-nitro-cGMP	8-nitro-cGMP	OFF	23396828

339	ABA=1	WT	8-nitro-cGMP	8-nitro-cGMP	ON	23396828
340	ABA=0	NO CA	some 8-nitro-cGMP, 8-nitro-cGMP	8-nitro-cGMP	Some/ON	23396828
341	ABA=1	NO KO	no 8-nitro-cGMP	8-nitro-cGMP	OFF	23396828
342	ABA=1	NOGC1 KO	no 8-nitro-cGMP	8-nitro-cGMP	OFF	23396828
343	ABA=1	NOGC1 KO, cGMP CA	8-nitro-cGMP	8-nitro-cGMP	ON	23396828
344	ABA=0	NO CA, NOGC1 KO	no 8-nitro-cGMP	8-nitro-cGMP	OFF	23396828
345	ABA=0	NO CA, NOGC1 KO, cGMP CA	8-nitro-cGMP	8-nitro-cGMP	ON	23396828
346	ABA=1	ROS KO	no 8-nitro-cGMP	8-nitro-cGMP	OFF	23396828
347	ABA=0	WT	no K^+ efflux	K^+ efflux	OFF	11027317
348	ABA=1	WT	K^+ efflux	K^+ efflux	ON	11027317
349	ABA=0	WT	no KEV	KEV	OFF	11027317
350	ABA=1	WT	KEV	KEV	ON	11027317
351	ABA=0	CaIM CA(Ca^{2+}_c oscillation)	some KEV, KEV	KEV	Some/ON	11027317
352	ABA=0	WT	no microtubule depolymerization	Microtubule Depolymerization	OFF	22402260, Qu et al.
353	ABA=1	WT	microtubule depolymerization	Microtubule Depolymerization	ON	22402260, Qu et al.
354	ABA=0	PLDα KO	no microtubule depolymerization	Microtubule Depolymerization	OFF	Qu et al.
355	ABA=1	PLDα KO	reduced microtubule depolymerization	Microtubule Depolymerization	Some	Qu et al.
356	ABA=0	PP2CA KO	no microtubule depolymerization	Microtubule Depolymerization	OFF	Qu et al.
357	ABA=1	PP2CA KO	microtubule depolymerization	Microtubule Depolymerization	ON	Qu et al.
358	ABA=0	PA CA	microtubule depolymerization	Microtubule Depolymerization	ON	Qu et al.
359	ABA=0	PA CA, PP2CA KO	some microtubule depolymerization, microtubule depolymerization	Microtubule Depolymerization	Some/ON	Qu et al.
360	ABA=0	Ca^{2+}_c KO	no microtubule depolymerization	Microtubule Depolymerization	OFF	24271006
361	ABA=1	Ca^{2+}_c KO	no, reduced microtubule depolymerization	Microtubule Depolymerization	OFF/Some	24271006
362	ABA=0	Ca^{2+}_c KO, PA CA	microtubule depolymerization	Microtubule Depolymerization	ON	24271006
363	ABA=0	Ca^{2+}_c KO, PLDα KO	no, some microtubule depolymerization	Microtubule Depolymerization	OFF/Some	24271006
364	ABA=1	Ca^{2+}_c KO, PLDα KO	no, reduced microtubule depolymerization	Microtubule Depolymerization	OFF/Some	24271006
365	ABA=0	Ca^{2+}_c KO, PA CA, PLDα KO	microtubule depolymerization	Microtubule Depolymerization	ON	24271006
366	ABA=0	CaIM CA	microtubule depolymerization	Microtubule Depolymerization	ON	24271006
367	ABA=0	CaIM CA, PLDα KO	some microtubule depolymerization	Microtubule Depolymerization	Some	24271006
368	ABA=0	WT	no vacuolar acidification	Vacuolar Acidification	OFF	23757398
369	ABA=1	WT	vacuolar acidification	Vacuolar Acidification	ON	23757398

370	ABA=0	PI3P5K KO	no vacuolar acidification	Vacuolar Acidification	OFF	23757398
371	ABA=1	PI3P5K KO	no, reduced vacuolar acidification	Vacuolar Acidification	OFF/Some	23757398
372	ABA=0	PI3P5K KO	no pH_c	pH_c	OFF	23757398
373	ABA=1	PI3P5K KO	no, reduced pH_c	pH_c	OFF/Some	23757398
374	ABA=0	V-PPase KO	no vacuolar acidification	Vacuolar Acidification	OFF	23757398
375	ABA=1	V-PPase KO	reduced vacuolar acidification	Vacuolar Acidification	Some	23757398
376	ABA=0	pH_c KO	no vacuolar acidification	Vacuolar Acidification	OFF	23757398
377	ABA=1	pH_c KO	no, reduced vacuolar acidification	Vacuolar Acidification	OFF/Some	23757398
378	ABA=0	pH_c KO	no ROS	ROS	OFF	15064385
379	ABA=1	pH_c KO	reduced ROS*	ROS	Some	15064385
380	ABA=0	OST1 KO	no CaIM	CaIM	OFF	24033256
381	ABA=1	OST1 KO	no CaIM	CaIM	OFF	24033256
382	ABA=0	OST1 CA	no CaIM	CaIM	OFF	24033256
383	ABA=1	OST1 CA	increased CaIM	CaIM	ON	24033256
384	ABA=0	OST1 KO	no ROS	ROS	OFF	24033256, 15064385
385	ABA=1	OST1 KO	no ROS	ROS	OFF	24033256, 15064385
386	ABA=0	OST1 CA	no ROS	ROS	OFF	24033256
387	ABA=1	OST1 CA	increased ROS	ROS	ON	24033256
388	ABA=0	RBOH KO	no ROS	ROS	OFF	15064385
389	ABA=1	RBOH KO	no ROS	ROS	OFF	15064385
390	ABA=0	OST1 KO, RBOH KO	no ROS	ROS	OFF	15064385
391	ABA=1	OST1 KO, RBOH KO	no ROS	ROS	OFF	15064385
392	ABA=0	KOUT KO, RBOH KO	no ROS	ROS	OFF	15064385
393	ABA=1	KOUT KO, RBOH KO	no ROS	ROS	OFF	15064385
394	ABA=0	ABI1 CA	no ROS	ROS	OFF	11701885, 19690149
395	ABA=1	ABI1 CA	no ROS /ROS	ROS	OFF	11701885 /19690149
396	ABA=0	ABI2 CA	no ROS	ROS	OFF	11701885
397	ABA=1	ABI2 CA	ROS	ROS	ON	11701885
398	ABA=0	ABI1 KO	no ROS	ROS	OFF	19690149
399	ABA=1	ABI1 KO	ROS	ROS	ON	19690149
400	ABA=0	PtdInsP3 KO	no ROS	ROS	OFF	12746515
401	ABA=1	PtdInsP3 KO	no, reduced ROS	ROS	OFF/Some	12746515
402	ABA=0	PtdInsP4 KO	no ROS	ROS	OFF	12746515
403	ABA=1	PtdInsP4 KO	ROS	ROS	ON	12746515
404	ABA=1	PtdInsP3 KO, PtdInsP4 KO	no ROS	ROS	OFF	12746515
405	ABA=0	PLDδ KO	no NO	NO	OFF	22932846
406	ABA=1	PLDδ KO	NO	NO	ON	22932846
407	ABA=0	PLDδ KO	no ROS	ROS	OFF	22932846

408	ABA=1	PLDδ KO	ROS reduced ROS, ROS	ROS	Some/ON	22932846, 22392280
409	ABA=0	WT	no PA	PA	OFF	19690149
410	ABA=1	WT	PA	PA	ON	19690149, 10518598, 22392280
411	ABA=0	PLDα KO	no PA	PA	OFF	19690149
412	ABA=1	PLDα KO	reduced PA	PA	Some	19690149, 22392280
413	ABA=0	PLDα KO	no, some ROS	ROS	OFF/Some	19690149
414	ABA=1	PLDα KO	no, reduced ROS reduced ROS	ROS	Some	19690149, 22392280
415	ABA=1	PLDα KO, PLDδ KO	no, reduced ROS	ROS	OFF/Some	22392280
416	ABA=0	PLDα KO	no NO	NO	OFF	19690149
417	ABA=1	PLDα KO	no NO	NO	OFF	19690149
418	ABA=1	PLDα KO, PLDδ KO	no NO	NO	OFF	22392280
419	ABA=0	PLDα KO, ROS CA	NO	NO	ON	19690149
420	ABA=0	WT	no AnionEM	AnionEM	OFF	19847112
421	ABA=1	WT	AnionEM	AnionEM	ON	19847112
422	ABA=0	cADPR KO	no AnionEM	AnionEM	OFF	19847112
423	ABA=1	cADPR KO	no AnionEM	AnionEM	OFF	19847112
424	ABA=0	PLC KO	no AnionEM	AnionEM	OFF	19847112
425	ABA=1	PLC KO	no AnionEM	AnionEM	OFF	19847112
426	ABA=1	WT	Depolarization	Depolarization	ON	19847112
427	ABA=1	cADPR KO	no Depolarization	Depolarization	OFF	19847112
428	ABA=1	PLC KO	no Depolarization	Depolarization	OFF	19847112
429	ABA=0	SACC KO, ERA1 KO	no CaIM	CaIM	OFF	12119381
430	ABA=1	SACC KO, ERA1 KO	increased CaIM	CaIM	ON	12119381
431	ABA=0	ERA1 KO	no SLAC1	SLAC1	OFF	12119381
432	ABA=1	ERA1 KO	SLAC1	SLAC1	ON	12119381
433	ABA=0	$Ca^{2+}{}_c$ KO	no QUAC1	QUAC1	OFF	23452338
434	ABA=1	$Ca^{2+}{}_c$ KO	QUAC1	QUAC1	ON	23452338
435	ABA=1	ABI1 CA, $Ca^{2+}{}_c$ KO	no QUAC1	QUAC1	OFF	23452338
436	ABA=1	$Ca^{2+}{}_c$ KO, OST1 KO	no QUAC1	QUAC1	OFF	23452338
437	ABA=1	PLDα KO, PLDδ KO	no PA	PA	OFF	10518598, 22392280
438	ABA=1	PLDδ KO	reduced PA	PA	Some	22392280
439	ABA=0	WT	no PLDα	PLDα	OFF	10518598
440	ABA=1	WT	reduced PLDα, PLDα	PLDα	Some/ON	10518598
441	ABA=0	WT	no PLDδ	PLDδ	OFF	10518598
442	ABA=1	WT	reduced PLDδ, PLDδ	PLDδ	Some/ON	10518598
443	ABA=1	WT	no, reduced DAG	DAG	OFF/Some	10518598
444	ABA=0	ROS CA	some SLAC1, SLAC1	SLAC1	Some/ON	22730405
445	ABA=0	OST1 KO, ROS CA	some SLAC1, SLAC1	SLAC1	Some/ON	22730405
446	ABA=0	GHR1 KO, ROS CA	no, some SLAC1	SLAC1	OFF/Some	22730405
447	ABA=0	SACC KO, ROS CA	some CaIM, CaIM	CaIM	Some/ON	21262908

448	ABA=0	SACC KO, GPA1 KO, ROS CA	some CaIM, CaIM	CaIM	Some/ON	21262908
449	ABA=0	S1P/PhytoS1P CA	$Ca^{2+}{}_c$ oscillation	$Ca^{2+}{}_c$	Some	11279499
450	ABA=0	CaIM CA	$Ca^{2+}{}_c$ oscillation	$Ca^{2+}{}_c$	Some	11429606
451	ABA=0	AtRAC1 KO	some actin reorganization, actin reorganization	Actin Reorganization	Some/ON	11459830
452	ABA=0	NO CA	some PA, PA	PA	Some/ON	17996010
453	ABA=0	PLC KO	no PA	PA	OFF	17996010
454	ABA=0	NO CA, PLC KO	no, some PA	PA	OFF/Some	17996010
455	ABA=0	ROS CA	some 8-nitro-cGMP, 8-nitro-cGMP	8-nitro-cGMP	Some/ON	23396828
456	ABA=0	ROS CA	some actin reorganization	Actin Reorganization	Some	18088331
457	ABA=0	CaIM CA	some SLAC1, SLAC1	SLAC1	Some/ON	19910530
458	ABA=0	MPK9/12 KO	no SLAC1	SLAC1	OFF	19910530
459	ABA=1	MPK9/12 KO	no SLAC1	SLAC1	OFF	19910530
460	ABA=0	CaIM CA, MPK9/12 KO	no SLAC1	SLAC1	OFF	19910530
461	ABA=0	PA CA	no $Ca^{2+}{}_c$	$Ca^{2+}{}_c$	OFF	10518598
462	ABA=0	GHR1 KO	no ROS	ROS	OFF	22730405
463	ABA=1	GHR1 KO	ROS	ROS	ON	22730405
464	ABA=0	ABI1 CA	no NO	NO	OFF	12446847, 19690149
465	ABA=1	ABI1 CA	NO	NO	ON	12446847, 19690149
466	ABA=0	ABI2 CA	no NO	NO	OFF	12446847
467	ABA=1	ABI2 CA	NO	NO	ON	12446847
468	ABA=0	PA CA	RBOH	RBOH	ON	19690149
469	ABA=0	PA CA	ROS some ROS (less than ABA=1)	ROS	Some/ON	19690149, 22392080
470	ABA=0	PA CA, PLDα KO, PLDδ KO	some ROS (less than ABA=1)	ROS	Some	22392080
471	ABA=0	PA CA	no NO	NO	OFF	22392080
472	ABA=0	PA CA, PLDα KO, PLDδ KO	no NO	NO	OFF	22392080
473	ABA=0	PA CA	pH_c	pH_c	ON	22392080
474	ABA=0	PA CA, PLDα KO, PLDδ KO	pH_c	pH_c	Some/ON	22392080
475	ABA=0	PC CA	no RBOH*	RBOH	OFF	19690149
476	ABA=0	PC CA	no ROS*	ROS	OFF	19690149
477	ABA=0	PA CA, RBOH KO	no ROS	ROS	OFF	19690149
478	ABA=0	WT	no OST1	OST1	OFF	26192964
479	ABA=1	WT	OST1	OST1	ON	26192964
480	ABA=0	ABI1 KO, ABI2 KO, HAB1 KO, PP2CA KO	no OST1	OST1	OFF	26192964
481	ABA=1	ABI1 KO, ABI2 KO, HAB1 KO, PP2CA KO	OST1	OST1	ON	26192964
482	ABA=0	CPK6 KO, CPK23 KO	no OST1	OST1	OFF	26192964
483	ABA=1	CPK6 KO, CPK23 KO	OST1	OST1	ON	26192964
484	ABA=0	CPK6 KO	no OST1	OST1	OFF	26192964
485	ABA=1	CPK6 KO	OST1	OST1	ON	26192964
486	ABA=0	WT	ABI1	ABI1	ON	19407143
487	ABA=1	WT	no ABI1	ABI1	OFF	19407143

488	ABA=0	WT	ABI2	ABI2	ON	19407143
489	ABA=1	WT	no ABI2	ABI2	OFF	19407143
490	ABA=0	WT	HAB1	HAB1	ON	19874541
491	ABA=1	WT	no HAB1	HAB1	OFF	19407142
492	ABA=0	WT	PP2CA	PP2CA	ON	22198272
493	ABA=1	WT	no PP2CA	PP2CA	OFF	22198272
494	ABA=0	WT	H^+ ATPase	H^+ ATPase	ON	15563626, 23946352
495	ABA=1	WT	no H^+ ATPase	H^+ ATPase	OFF	15563626, 23946352
496	ABA=0	WT	Malate	Malate	ON	12392716
497	ABA=1	WT	no Malate	Malate	OFF	24419583
498	ABA=0	WT	no InsP3	InsP3	OFF	12226236
499	ABA=1	WT	InsP3	InsP3	ON	12226236
500	ABA=0	WT	no S1P/PhytoS1P	S1P/PhytoS1P	OFF	12789341
501	ABA=1	WT	S1P/PhytoS1P	S1P/PhytoS1P	ON	12789341
502	ABA=0	WT	no SPHK1/2	SPHK1/2	OFF	12789341
503	ABA=1	WT	SPHK1/2	SPHK1/2	ON	12789341
504	ABA=0	WT	no RCARs	RCARs	OFF	19874541
505	ABA=1	WT	RCARs	RCARs	ON	19874541

S5 Table. Summary of the scores and features of the genetic algorithm-modified models as compared to the original 2017 model of ABA-induced stomatal closure.

The name of each model that was refined through the genetic algorithm starts with GA. “VA-KEV del” refers to the 2017 model corrected by deleting an erroneous edge that targets KEV. “GA - VA-KEV del” represents the outcome of the genetic algorithm when starting from the VA-KEV del model. Li (2006) refers to the earliest version of the model of ABA-induced stomatal closure [28]. Waidyarathne (2018) [41] is a model that builds on and expands the Li et al. model. Maheshwari (2019) [30] is a follow-up to the 2017 model. Baseline-A represents the corrected 2017 model (VA-KEV del) augmented with a self-edge on H_2O efflux. Baseline-B represents the model that replaces the $Ca^{2+}{}_c$ and Ca^{2+} ATPase nodes with a merged Ca2+osc node. The GA0 models are GA-improved versions of the respective baselines but without allowing additional edges. The GA1 models allow the addition of edges from a pool of 13 experimentally-supported edges. The GA2 models start from the respective GA1 model and allow the addition of 8 more edges.

Model	Score	Notes
Albert (2017)	310.5 / 505 (61.5%)	wrong regulatory edge for KEV
VA-KEV del	291.7 / 505 (57.8%)	failed to achieve ABA induced closure
GA - VA-KEV del	385.3 / 505 (76.3%)	failed to achieve ABA induced closure
Li (2006)	129.8 / 248 (52.3%)	39 nodes shared with the 2017 model
Waidyarathne (2018)	175.8 / 296 (59.4%)	49 nodes shared with the 2017 model
Maheshwari (2019)	240.0 / 385 (62.3%)	47 nodes shared with the 2017 model
baseline-A	311.7 / 505 (61.7%)	
baseline-B	184.2 / 505 (36.5%)	alternate Ca^{2+} representation
GA0-A	390.8 / 505 (77.4%)	no extra edges
GA0-B	384.6 / 505 (76.2%)	no extra edges, alternate Ca^{2+} representation
GA1-A	426.9 / 505 (84.5%)	

GA1-B	407.9 / 505 (80.8%)	alternate Ca^{2+} representation
GA2-A	431.2 / 505 (85.4%)	more assumed edges, started from GA1-A
GA2-B	412.8 / 505 (81.7%)	alternate Ca^{2+} representation, more assumed edges, started from GA1-B

References

1. Abou-Jaoudé W, Traynard P, Monteiro PT, Saez-Rodriguez J, Helikar T, Thieffry D, et al. Logical Modeling and Dynamical Analysis of Cellular Networks. Front Genet. 2016;7: 94.

2. McCulloch WS, Pitts W. A logical calculus of the ideas immanent in nervous activity. Bull Math Biophys. 1943;5: 115–133.

3. Hopfield JJ. Neural networks and physical systems with emergent collective computational abilities. Proc Natl Acad Sci U S A. 1982;79: 2554–2558.

4. Castellano C, Fortunato S, Loreto V. Statistical physics of social dynamics. Rev Mod Phys. 2009;81: 591–646.

5. Campbell C, Yang S, Albert R, Shea K. A network model for plant-pollinator community assembly. Proc Natl Acad Sci U S A. 2011;108: 197–202.

6. Park KH, Costa FX, Rocha LM, Albert R, Rozum JC. Robustness of biomolecular networks suggests functional modules far from the edge of chaos. bioRxiv. 2023. p. 2023.06.30.547297. doi:10.1101/2023.06.30.547297

7. Zañudo JGT, Albert R. An effective network reduction approach to find the dynamical repertoire of discrete dynamic networks. Chaos. 2013;23: 025111.

8. Rozum JC, Gómez Tejeda Zañudo J, Gan X, Deritei D, Albert R. Parity and time reversal elucidate both decision-making in empirical models and attractor scaling in critical Boolean networks. Sci Adv. 2021;7. doi:10.1126/sciadv.abf8124

9. Deritei D, Rozum J, Ravasz Regan E, Albert R. A feedback loop of conditionally stable circuits drives the cell cycle from checkpoint to checkpoint. Sci Rep. 2019;9: 16430.

10. Rozum JC, Deritei D, Park KH, Zañudo JGT, Albert R. pystablemotifs: Python library for attractor identification and control in Boolean networks. Bioinformatics. 2021. doi:10.1093/bioinformatics/btab825

11. Veitia RA. A sigmoidal transcriptional response: cooperativity, synergy and dosage effects. Biol Rev Camb Philos Soc. 2003;78: 149–170.

12. Tyson JJ, Chen KC, Novak B. Sniffers, buzzers, toggles and blinkers: dynamics of regulatory and signaling pathways in the cell. Curr Opin Cell Biol. 2003;15: 221–231.

13. Martinez-Sanchez ME, Mendoza L, Villarreal C, Alvarez-Buylla ER. A Minimal Regulatory Network of Extrinsic and Intrinsic Factors Recovers Observed Patterns of CD4+ T Cell Differentiation and Plasticity. PLoS Comput Biol. 2015;11: e1004324.

14. Steinway SN, Zañudo JGT, Michel PJ, Feith DJ, Loughran TP, Albert R. Combinatorial interventions inhibit TGFβ-driven epithelial-to-mesenchymal transition and support hybrid cellular phenotypes. NPJ Syst Biol Appl. 2015;1: 15014.

15. Rodríguez-Jorge O, Kempis-Calanis LA, Abou-Jaoudé W, Gutiérrez-Reyna DY, Hernandez C, Ramirez-Pliego O, et al. Cooperation between T cell receptor and Toll-like receptor 5 signaling for CD4+ T cell activation. Sci Signal. 2019;12. doi:10.1126/scisignal.aar3641

16. Gómez Tejeda Zañudo J, Mao P, Alcon C, Kowalski K, Johnson GN, Xu G, et al. Cell Line–Specific Network Models of ER+ Breast Cancer Identify Potential PI3Kα Inhibitor Resistance Mechanisms and Drug Combinations. Cancer Res. 2021;81: 4603–4617.

17. Klarner H, Streck A, Siebert H. PyBoolNet: a python package for the generation, analysis and visualization of boolean networks. Bioinformatics. 2017;33: 770–772.

18. Beneš N, Brim L, Huvar O, Pastva S, Šafránek D, Šmijáková E. AEON.py: Python library for attractor analysis in asynchronous Boolean networks. Bioinformatics. 2022;38: 4978–4980.

19. Trinh V-G, Benhamou B, Soliman S. Trap spaces of Boolean networks are conflict-free siphons of their Petri net encoding. Theor Comput Sci. 2023;971: 114073.

20. Trinh H-C, Kwon Y-K. A novel constrained genetic algorithm-based Boolean network inference method from steady-state gene expression data. Bioinformatics. 2021;37: i383–i391.

21. Dorier J, Crespo I, Niknejad A, Liechti R, Ebeling M, Xenarios I. Boolean regulatory network reconstruction using literature based knowledge with a genetic algorithm optimization method. BMC Bioinformatics. 2016;17: 410.

22. Ghaffarizadeh A, Podgorski GJ, Flann NS. Applying attractor dynamics to infer gene regulatory interactions involved in cellular differentiation. Biosystems. 2017;155: 29–41.

23. Müssel C, Ikonomi N, Werle SD, Weidner FM, Maucher M, Schwab JD, et al. CANTATA-prediction of missing links in Boolean networks using genetic programming. Bioinformatics. 2022;38: 4893–4900.

24. Palli R, Palshikar MG, Thakar J. Executable pathway analysis using ensemble discrete-state modeling for large-scale data. PLoS Comput Biol. 2019;15: e1007317.

25. Muñoz S, Carrillo M, Azpeitia E, Rosenblueth DA. Griffin: A Tool for Symbolic Inference of Synchronous Boolean Molecular Networks. Front Genet. 2018;9: 39.

26. Mendoza L. A network model for the control of the differentiation process in Th cells. Biosystems. 2006;84: 101–114.

27. Mendoza L, Pardo F. A robust model to describe the differentiation of T-helper cells. Theory Biosci. 2010;129: 283–293.

28. Li S, Assmann SM, Albert R. Predicting essential components of signal transduction networks: a dynamic model of guard cell abscisic acid signaling. PLoS Biol. 2006;4: e312.

29. Albert R, Acharya BR, Jeon BW, Zañudo JGT, Zhu M, Osman K, et al. A new discrete dynamic model of ABA-induced stomatal closure predicts key feedback loops. PLoS Biol. 2017;15: e2003451.

30. Maheshwari P, Du H, Sheen J, Assmann SM, Albert R. Model-driven discovery of calcium-related protein-phosphatase inhibition in plant guard cell signaling. PLoS Comput Biol. 2019;15: e1007429.

31. Maheshwari P, Assmann SM, Albert R. A Guard Cell Abscisic Acid (ABA) Network Model That Captures the Stomatal Resting State. Front Physiol. 2020;11: 927.

32. Park S-Y, Fung P, Nishimura N, Jensen DR, Fujii H, Zhao Y, et al. Abscisic acid inhibits type 2C protein phosphatases via the PYR/PYL family of START proteins. Science. 2009;324: 1068–1071.

33. Santiago J, Rodrigues A, Saez A, Rubio S, Antoni R, Dupeux F, et al. Modulation of drought resistance by the abscisic acid receptor PYL5 through inhibition of clade A PP2Cs. Plant J. 2009;60: 575–588.

34. Weiner JJ, Peterson FC, Volkman BF, Cutler SR. Structural and functional insights into core ABA signaling. Curr Opin Plant Biol. 2010;13: 495–502.

35. Mitchell M. An introduction to genetic algorithms mit press. Cambridge, Massachusetts London, England.

36. Terfve C, Cokelaer T, Henriques D, MacNamara A, Goncalves E, Morris MK, et al. CellNOptR: a flexible toolkit to train protein signaling networks to data using multiple logic formalisms. BMC Syst Biol. 2012;6: 133.

37. Gouveia F, Lynce I, Monteiro PT. Revision of Boolean Models of Regulatory Networks Using Stable State Observations. J Comput Biol. 2020;27: 144–155.

38. Aleixo F, Knorr M, Leite J. Revising Boolean logical models of biological regulatory networks. Proceedings of the Twentieth International Conference on Principles of Knowledge Representation and Reasoning. California: International Joint Conferences on Artificial Intelligence Organization; 2023. pp. 12–22.

39. Azpeitia E, Weinstein N, Benítez M, Mendoza L, Alvarez-Buylla ER. Finding Missing Interactions of the Arabidopsis thaliana Root Stem Cell Niche Gene Regulatory Network. Front Plant Sci. 2013;4: 110.

40. Helikar T, Kowal B, McClenathan S, Bruckner M, Rowley T, Madrahimov A, et al. The Cell Collective: toward an open and collaborative approach to systems biology. BMC Syst Biol. 2012;6: 96.

41. Waidyarathne P, Samarasinghe S. Boolean Calcium Signalling Model Predicts Calcium Role in Acceleration and Stability of Abscisic Acid-Mediated Stomatal Closure. Sci Rep. 2018;8: 17635.

42. Mcainsh MR. Calcium Oscillations in Guard Cell Adaptive Responses to the Environment. In: Mancuso S, Shabala S, editors. Rhythms in Plants: Phenomenology, Mechanisms, and Adaptive Significance. Berlin, Heidelberg: Springer Berlin Heidelberg; 2007. pp. 135–155.

43. Maheshwari P, Assmann SM, Albert R. Inference of a Boolean Network From Causal Logic Implications. Front Genet. 2022;13: 836856.

44. Allen GJ, Chu SP, Harrington CL, Schumacher K, Hoffmann T, Tang YY, et al. A defined range of guard cell calcium oscillation parameters encodes stomatal movements. Nature. 2001;411: 1053–1057.

45. Hsu P-K, Dubeaux G, Takahashi Y, Schroeder JI. Signaling mechanisms in abscisic acid-mediated stomatal closure. Plant J. 2021;105: 307–321.

46. Schwartz A. Role of Ca and EGTA on Stomatal Movements in Commelina communis L.

Plant Physiol. 1985;79: 1003–1005.

47. Rodrigues O, Reshetnyak G, Grondin A, Saijo Y, Leonhardt N, Maurel C, et al. Aquaporins facilitate hydrogen peroxide entry into guard cells to mediate ABA- and pathogen-triggered stomatal closure. Proc Natl Acad Sci U S A. 2017;114: 9200–9205.

48. Eisinger W, Ehrhardt D, Briggs W. Microtubules are essential for guard-cell function in Vicia and Arabidopsis. Mol Plant. 2012;5: 601–610.

49. Bright J, Desikan R, Hancock JT, Weir IS, Neill SJ. ABA-induced NO generation and stomatal closure in Arabidopsis are dependent on H2O2 synthesis. Plant J. 2006;45: 113–122.

50. Yang H-M, Zhang J-H, Zhang X-Y. Regulation mechanisms of stomatal oscillation. J Integr Plant Biol. 2005;47: 1159–1172.

51. Emmert-Streib F, Dehmer M, Haibe-Kains B. Gene regulatory networks and their applications: understanding biological and medical problems in terms of networks. Front Cell Dev Biol. 2014;2: 38.

52. Nguyen H, Tran D, Tran B, Pehlivan B, Nguyen T. A comprehensive survey of regulatory network inference methods using single cell RNA sequencing data. Brief Bioinform. 2021;22. doi:10.1093/bib/bbaa190

53. Pillich RT, Chen J, Churas C, Liu S, Ono K, Otasek D, et al. NDEx: Accessing Network Models and Streamlining Network Biology Workflows. Curr Protoc. 2021;1: e258.

54. Licata L, Lo Surdo P, Iannuccelli M, Palma A, Micarelli E, Perfetto L, et al. SIGNOR 2.0, the SIGnaling Network Open Resource 2.0: 2019 update. Nucleic Acids Res. 2020;48: D504–D510.

55. Milacic M, Beavers D, Conley P, Gong C, Gillespie M, Griss J, et al. The Reactome Pathway Knowledgebase 2024. Nucleic Acids Res. 2023. doi:10.1093/nar/gkad1025

56. Everitt BS, Skrondal A. The Cambridge Dictionary of Statistics. Cambridge University Press; 2010.

57. Gan X, Albert R. General method to find the attractors of discrete dynamic models of biological systems. Phys Rev E. 2018;97: 042308.

58. Holtzapple E, Telmer CA, Miskov-Zivanov N. FLUTE: Fast and reliable knowledge retrieval from biomedical literature. Database . 2020;2020. doi:10.1093/database/baaa056

59. Ahmed Y, Telmer CA, Miskov-Zivanov N. CLARINET: efficient learning of dynamic network models from literature. Bioinformatics Advances. 2021;1: vbab006.

60. Chatain T, Haar S, č, Paulevé L. Most Permissive Semantics of Boolean Networks. arXiv [cs.FL]. 2018. Available: http://arxiv.org/abs/1808.10240

61. Saez-Rodriguez J, Alexopoulos LG, Epperlein J, Samaga R, Lauffenburger DA, Klamt S, et al. Discrete logic modelling as a means to link protein signalling networks with functional analysis of mammalian signal transduction. Mol Syst Biol. 2009;5: 331.

62. Sayed K, Bocan KN, Miskov-Zivanov N. Automated Extension of Cell Signaling Models with Genetic Algorithm. 2018 40th Annual International Conference of the IEEE Engineering in Medicine and Biology Society (EMBC). 2018. pp. 5030–5033.

63. Helikar T, Konvalina J, Heidel J, Rogers JA. Emergent decision-making in biological signal transduction networks. Proc Natl Acad Sci U S A. 2008;105: 1913–1918.

64. Qu Y, Song P, Hu Y, Jin X, Jia Q, Zhang X, et al. Regulation of stomatal movement by cortical microtubule organization in response to darkness and ABA signaling in Arabidopsis. Plant Growth Regul. 2018;84: 467–479.

65. Postiglione AE, Muday GK. The Role of ROS Homeostasis in ABA-Induced Guard Cell Signaling. Front Plant Sci. 2020;11: 968.

66. Grondin A, Rodrigues O, Verdoucq L, Merlot S, Leonhardt N, Maurel C. Aquaporins Contribute to ABA-Triggered Stomatal Closure through OST1-Mediated Phosphorylation. Plant Cell. 2015;27: 1945–1954.

67. Li X, Li J-H, Wang W, Chen N-Z, Ma T-S, Xi Y-N, et al. ARP2/3 complex-mediated actin dynamics is required for hydrogen peroxide-induced stomatal closure in Arabidopsis. Plant Cell Environ. 2014;37: 1548–1560.

68. Choi Y, Lee Y, Jeon BW, Staiger CJ, Lee Y. Phosphatidylinositol 3- and 4-phosphate modulate actin filament reorganization in guard cells of day flower. Plant Cell Environ. 2008;31: 366–377.

69. Yang Y, Zhao Y, Zheng W, Zhao Y, Zhao S, Wang Q, et al. Phosphatidylinositol 3-phosphate regulates SCAB1-mediated F-actin reorganization during stomatal closure in Arabidopsis. Plant Cell. 2022;34: 477–494.

70. Jiang Y, Wu K, Lin F, Qu Y, Liu X, Zhang Q. Phosphatidic acid integrates calcium signaling and microtubule dynamics into regulating ABA-induced stomatal closure in Arabidopsis. Planta. 2014;239: 565–575.

71. Bak G, Lee E-J, Lee Y, Kato M, Segami S, Sze H, et al. Rapid structural changes and acidification of guard cell vacuoles during stomatal closure require phosphatidylinositol 3,5-bisphosphate. Plant Cell. 2013;25: 2202–2216.

72. Li Z, Takahashi Y, Scavo A, Brandt B, Nguyen D, Rieu P, et al. Abscisic acid-induced degradation of Arabidopsis guanine nucleotide exchange factor requires calcium-dependent protein kinases. Proc Natl Acad Sci U S A. 2018;115: E4522–E4531.

73. Sierla M, Hõrak H, Overmyer K, Waszczak C, Yarmolinsky D, Maierhofer T, et al. The Receptor-like Pseudokinase GHR1 Is Required for Stomatal Closure. Plant Cell. 2018;30: 2813–2837.

74. Lee Y, Choi YB, Suh S, Lee J, Assmann SM, Joe CO, et al. Abscisic Acid-Induced Phosphoinositide Turnover in Guard Cell Protoplasts of Vicia faba. Plant Physiol. 1996;110: 987–996.

75. Jacob T, Ritchie S, Assmann SM, Gilroy S. Abscisic acid signal transduction in guard cells is mediated by phospholipase D activity. Proc Natl Acad Sci U S A. 1999;96: 12192–12197.

76. Zhang W, Jeon BW, Assmann SM. Heterotrimeric G-protein regulation of ROS signalling and calcium currents in Arabidopsis guard cells. J Exp Bot. 2011;62: 2371–2379.

77. Mishra G, Zhang W, Deng F, Zhao J, Wang X. A bifurcating pathway directs abscisic acid effects on stomatal closure and opening in Arabidopsis. Science. 2006;312: 264–266.

78. Desikan R, Griffiths R, Hancock J, Neill S. A new role for an old enzyme: nitrate reductase-mediated nitric oxide generation is required for abscisic acid-induced stomatal closure in Arabidopsis thaliana. Proc Natl Acad Sci U S A. 2002;99: 16314–16318.

79. MacRobbie EAC. ABA activates multiple Ca2+ fluxes in stomatal guard cells, triggering vacuolar K+(Rb+) release. Proceedings of the National Academy of Sciences. 2000;97: 12361–12368.

80. Zhao Y, Zhao S, Mao T, Qu X, Cao W, Zhang L, et al. The plant-specific actin binding protein SCAB1 stabilizes actin filaments and regulates stomatal movement in Arabidopsis. Plant Cell. 2011;23: 2314–2330.

81. Joudoi T, Shichiri Y, Kamizono N, Akaike T, Sawa T, Yoshitake J, et al. Nitrated cyclic GMP modulates guard cell signaling in Arabidopsis. Plant Cell. 2013;25: 558–571.

82. Meyer S, Mumm P, Imes D, Endler A, Weder B, Al-Rasheid KAS, et al. AtALMT12 represents an R-type anion channel required for stomatal movement in Arabidopsis guard cells. Plant J. 2010;63: 1054–1062.

83. Imes D, Mumm P, Böhm J, Al-Rasheid KAS, Marten I, Geiger D, et al. Open stomata 1 (OST1) kinase controls R-type anion channel QUAC1 in Arabidopsis guard cells. Plant J. 2013;74: 372–382.

84. Geiger D, Maierhofer T, Al-Rasheid KAS, Scherzer S, Mumm P, Liese A, et al. Stomatal closure by fast abscisic acid signaling is mediated by the guard cell anion channel SLAH3 and the receptor RCAR1. Sci Signal. 2011;4: ra32.

85. Vahisalu T, Kollist H, Wang Y-F, Nishimura N, Chan W-Y, Valerio G, et al. SLAC1 is required for plant guard cell S-type anion channel function in stomatal signalling. Nature. 2008;452: 487–491.